The IQD Family of Calmodulin-Binding Proteins Links Calcium Signaling to Microtubules, Membrane Subdomains, and the Nucleus[1][OPEN]

Katharina Bürstenbinder*, Birgit Möller, Romina Plötner, Gina Stamm, Gerd Hause, Dipannita Mitra, and Steffen Abel

Department of Molecular Signal Processing, Leibniz Institute of Plant Biochemistry, 06120 Halle (Saale), Germany (K.B., R.P., G.S., D.M., S.A.); Institute of Computer Science (B.M.), Biocenter (G.H.), and Institute of Biochemistry and Biotechnology (S.A.), Martin Luther University Halle-Wittenberg, 06120 Halle (Saale), Germany; and Department of Plant Sciences, University of California, Davis, California 95616 (S.A.)

ORCID IDs: 0000-0002-3493-4800 (K.B.); 0000-0002-7146-043X (B.M.).

Calcium (Ca^{2+}) signaling and dynamic reorganization of the cytoskeleton are essential processes for the coordination and control of plant cell shape and cell growth. Calmodulin (CaM) and closely related calmodulin-like (CML) polypeptides are principal sensors of Ca^{2+} signals. CaM/CMLs decode and relay information encrypted by the second messenger via differential interactions with a wide spectrum of targets to modulate their diverse biochemical activities. The plant-specific IQ67 DOMAIN (IQD) family emerged as possibly the largest class of CaM-interacting proteins with undefined molecular functions and biological roles. Here, we show that the 33 members of the IQD family in Arabidopsis (*Arabidopsis thaliana*) differentially localize, using green fluorescent protein (GFP)-tagged proteins, to multiple and distinct subcellular sites, including microtubule (MT) arrays, plasma membrane subdomains, and nuclear compartments. Intriguingly, the various IQD-specific localization patterns coincide with the subcellular patterns of IQD-dependent recruitment of CaM, suggesting that the diverse IQD members sequester Ca^{2+}-CaM signaling modules to specific subcellular sites for precise regulation of Ca^{2+}-dependent processes. Because MT localization is a hallmark of most IQD family members, we quantitatively analyzed GFP-labeled MT arrays in *Nicotiana benthamiana* cells transiently expressing GFP-IQD fusions and observed IQD-specific MT patterns, which point to a role of IQDs in MT organization and dynamics. Indeed, stable overexpression of select IQD proteins in Arabidopsis altered cellular MT orientation, cell shape, and organ morphology. Because IQDs share biochemical properties with scaffold proteins, we propose that IQD families provide an assortment of platform proteins for integrating CaM-dependent Ca^{2+} signaling at multiple cellular sites to regulate cell function, shape, and growth.

Calcium (Ca^{2+}), a general second messenger in all eukaryotes, is required for the execution of developmental programs and the coordination of numerous adaptive responses to external cues, complex processes necessitating a precise regulation of cell growth, and cell shape (Cárdenas, 2009; Steinhorst and Kudla, 2013). Cellular Ca^{2+} oscillations are monitored by polydentate Ca^{2+} sensors, such as calmodulin (CaM) and calmodulin-like (CML) polypeptides, which differentially interact upon Ca^{2+} binding with a broad range of diverse proteins to modulate their biochemical activities (McCormack and Braam, 2003; McCormack et al., 2005). An extra layer of complexity is added by Ca^{2+}-free apo-CaM that regulates a largely different subset of cellular targets (Jurado et al., 1999). Fundamental processes affected by Ca^{2+} and CaM/CMLs include, among others, transcriptional reprogramming, regulation of metabolism, or the control of cell division and polarity (Hepler, 2005).

The microtubule (MT) cytoskeleton forms a highly dynamic network and plays a central role for coordinating cell growth. Cortical MT arrays are attached to the plasma membrane (PM) for structural support (Liu et al., 2015) and determine the direction of cell expansion by guiding cellulose synthase complexes (CSCs; Endler and Persson, 2011). Furthermore, the MT cytoskeleton mediates the intracellular transport of diverse cargoes (Lloyd and Hussey, 2001; Sedbrook and Kaloriti, 2008) and contributes to exocytosis (Zárský et al., 2009; Idilli et al., 2013; Kong et al., 2015; Zhu et al., 2015a). To generate the various MT arrays, networks of microtubule-associated

[1] This work was supported by the Collaborative Research Center of the Deutsche Forschungsgemeinschaft (grant no. SFB 648; project B12 to K.B., R.P., and S.A. and project Z1 to G.H.), by the German Academic Exchange Service (to D.M.), and by core funding (Leibniz Association) from the Federal Republic of Germany and the state of Saxony-Anhalt.

* Address correspondence to katharina.buerstenbinder@ipb-halle.de.

The author responsible for distribution of materials integral to the findings presented in this article in accordance with the policy described in the Instructions for Authors (www.plantphysiology.org) is: Katharina Bürstenbinder (katharina.buerstenbinder@ipb-halle.de).

K.B. and S.A. designed the research; B.M. and K.B. analyzed microtubule patterns and quantified cell shape characteristics; G.H. performed electron microscopy experiments; K.B., G.S., R.P., and D.M. performed all other experiments and analyzed the data; K.B. wrote the article; S.A. edited the article.

[OPEN] Articles can be viewed without a subscription.

www.plantphysiol.org/cgi/doi/10.1104/pp.16.01743

proteins (MAPs) control MT dynamics, stability, and organization (Gardiner, 2013; Struk and Dhonukshe, 2014). MAPs also connect CSCs to MTs and are thought to tether cortical MTs to the PM (Endler and Persson, 2011; Bringmann et al., 2012; Liu et al., 2016). Several studies implicated Ca^{2+}-CaM signaling in the control of cytoskeleton organization and dynamics (Hepler, 2016). For example, in yeast and animals, Ras GTPase-activating-like protein IQGAP (IQGAP) scaffold proteins, which recruit CaM via IQ motifs and feature a domain related to GTPase-activating proteins, are key regulators of the cytoskeleton (Shannon, 2012). IQGAPs contribute to the regulation of cell-to-cell contact and coordinate intracellular signaling from membranes to the nucleus (Smith et al., 2015). However, plant genomes do not encode IQGAPs, and the mechanisms of Ca^{2+}-mediated cytoskeletal organization are largely elusive (Hepler, 1992, 2005; Wang et al., 2011). During the colonization of terrestrial habitats, novel adaptive traits evolved in land plants (Graham, 1996), and the size of plant CaM/CML families expanded greatly to provide versatility for transducing complex Ca^{2+} signals into numerous cellular and environmental responses (McCormack et al., 2005; Zhu et al., 2015b). Likewise, the cytoskeleton acquired additional functions for adapting cell shape and cell growth, and a multitude of unique MAPs emerged for generating the various cytoskeletal arrays and controlling their organization and stability (Gardiner, 2013; Struk and Dhonukshe, 2014). Therefore, it is likely that signaling scaffolds analogous to IQGAP proteins evolved in plants for Ca^{2+}-CaM-dependent regulation of the cytoskeleton.

To elucidate CaM-mediated Ca^{2+} signaling in plants, extensive efforts have been made to identify CaM/CML-binding proteins (CaMBPs). More than 300 CaMBPs are currently known, which include transporters and channels, metabolic enzymes, transcription factors, myosins, and various proteins of undefined functions that mostly interact with either holo-CaM or apo-CaM (Reddy et al., 2011). To date, only one CaM-binding MAP has been reported, KINESIN-LIKE CaM-BINDING PROTEIN/ZWICHEL (KCBP/ZWI; Narasimhulu and Reddy, 1998), which functions in trichome development (Hülskamp et al., 1994; Oppenheimer et al., 1997; Tian et al., 2015) and root growth (Buschmann et al., 2015; Humphrey et al., 2015). During cell division, KCBP localizes to the cortical division zone and likely functions in phragmoplast guidance and in the spatial control of cytokinesis (Buschmann et al., 2015). The activity of KCBP/ZWI is regulated by Ca^{2+}-CaM (Kao et al., 2000), and CaM binding abolishes MT interaction of its motor domain (Deavours et al., 1998; Narasimhulu and Reddy, 1998). Because not all effects of CaM/CMLs on MT arrays may be explained by KCBP action, additional players likely are required for the CaM-dependent regulation of MT organization and dynamics (Hepler, 2016).

The IQ67 DOMAIN (IQD) family of mostly uncharacterized plant-specific CaMBPs may represent such candidates at the nexus of Ca^{2+} signaling and cell growth control. IQD proteins are defined by their characteristic IQ domain of 67 conserved amino acid residues, which harbors three different consensus CaM recruitment motifs in a unique and repetitive arrangement, including up to three copies of the IQ motif (Abel et al., 2013). The IQ67 domain is sufficient and required for CaM interaction in vitro, and the founding member, Arabidopsis (*Arabidopsis thaliana*) IQD1 (Levy et al., 2005), localizes to MT arrays and the cell nucleus (Bürstenbinder et al., 2013). The 33 IQD proteins of Arabidopsis are highly diverse in length (103–794 amino acids) and cluster in four major phylogenetic clades that differ mainly in the presence and distribution of family-specific motifs flanking the central IQ67 domain (Abel et al., 2005). Extensive *IQD* families (23–67 genes) have been annotated in rice (*Oryza sativa*; Abel et al., 2005) and recently in purple falsebrome (*Brachypodium distachyon*; Filiz et al., 2013), tomato (*Solanum lycopersicum*; Huang et al., 2013), soybean (*Glycine max*; Feng et al., 2014), poplar (*Populus trichocarpa*; Ma et al., 2014), and moso bamboo (*Phyllostachys edulis*; Wu et al., 2016). Thus, IQD proteins are possibly the largest class of CaMBPs in plants; however, their precise biological roles and biochemical functions remain to be elucidated (Abel et al., 2013; van der Knaap et al., 2014). Coexpression assays demonstrated that IQD1 colocalizes with CaM2 to MT arrays (Bürstenbinder et al., 2013), which suggests a role for IQD1 in linking Ca^{2+}-CaM signaling to the regulation of MT-associated processes (Abel et al., 2013). Additional support for IQD functions at MTs is indirectly provided by studies in tomato, which showed that duplication of the *IQD12/SUN* locus causes elongated fruits, altered cell shape, and twisted stems (Xiao et al., 2008; Wu et al., 2011). These phenotypes are reminiscent of plants with mutations in tubulin subunits (Ishida et al., 2007) and several MAPs (Buschmann et al., 2004; Sedbrook et al., 2004). Collectively, the limited evidence points to regulatory roles of IQD proteins in Ca^{2+}-CaM signaling and plant development.

Here, we present, to our knowledge, the first comprehensive characterization of the entire Arabidopsis IQD family. The 33 IQD proteins differentially localize to multiple subcellular sites, including MTs, the PM, and nuclear compartments. As demonstrated for eight representative IQD family members, the specific IQD localization patterns coincide with the subcellular patterns of IQD-dependent CaM recruitment. Misexpression of select IQD proteins alters the cell shape and pattern of MT organization. Thus, the prospect arises that the plant-specific IQD families provide an assortment of scaffold-like proteins to sequester and integrate CaM-dependent Ca^{2+} signaling at multiple subcellular sites to regulate cell function, shape, and growth.

RESULTS

IQD Family Members Differentially Localize to MTs, Membranes, and the Nucleus

To gain insights into the cellular sites of IQD function, we studied the subcellular distribution of all 33 Arabidopsis

IQD family members after transient expression in *Nicotiana benthamiana* leaves, which is a convenient system in which to monitor protein localization (Deeks et al., 2012). We expressed GFP-tagged IQDs under the control of the cauliflower mosaic virus (*CaMV*) *35S* promoter to facilitate their detection. The authentic GFP reporter was included as a reference, which uniformly labeled the cytoplasm and cell nucleus with the exception of its nucleolus (Fig. 1, bottom right). We confirmed the expression of all full-length IQD fusion proteins by immunoblot analysis using an anti-GFP antibody (Supplemental Fig. S1A). N-terminal GFP fusions of most IQD proteins were associated at least partially with cytoskeletal arrays (Fig. 1). Localization to the MT cytoskeleton was confirmed by coexpression with red fluorescent protein (RFP)-TUBULIN ALPHA5 (TUA5), a marker for MTs (Gutierrez et al., 2009), as shown for GFP-IQD1 (Fig. 1), GFP-IQD13, and GFP-IQD16 (Supplemental Fig. S1B). About half of the GFP-tagged IQD family members labeled the PM (e.g. IQD12, IQD22, and IQD25) or the nuclear envelope (e.g. IQD8 and IQD27). In addition, several GFP-IQD fusions localized to the nucleus (e.g. IQD10, IQD28, and IQD32), nucleolus (e.g. IQD3, IQD4, and IQD20), or distinct nuclear bodies (e.g. IQD6, IQD9, and IQD24; Fig. 1, insets). Their translocation into the nucleus is likely an active process because the size of most GFP-IQD fusions exceeds the exclusion limit (greater than 50–60 kD) of nuclear pores (Nigg, 1997), and most nucleus-localized IQD proteins contain predicted nuclear localization signals (Supplemental Table S1). The smallest family member, IQD20, lacks a nuclear localization signal; thus, its GFP fusion (38.7 kD) is capable of passive diffusion into the nucleus.

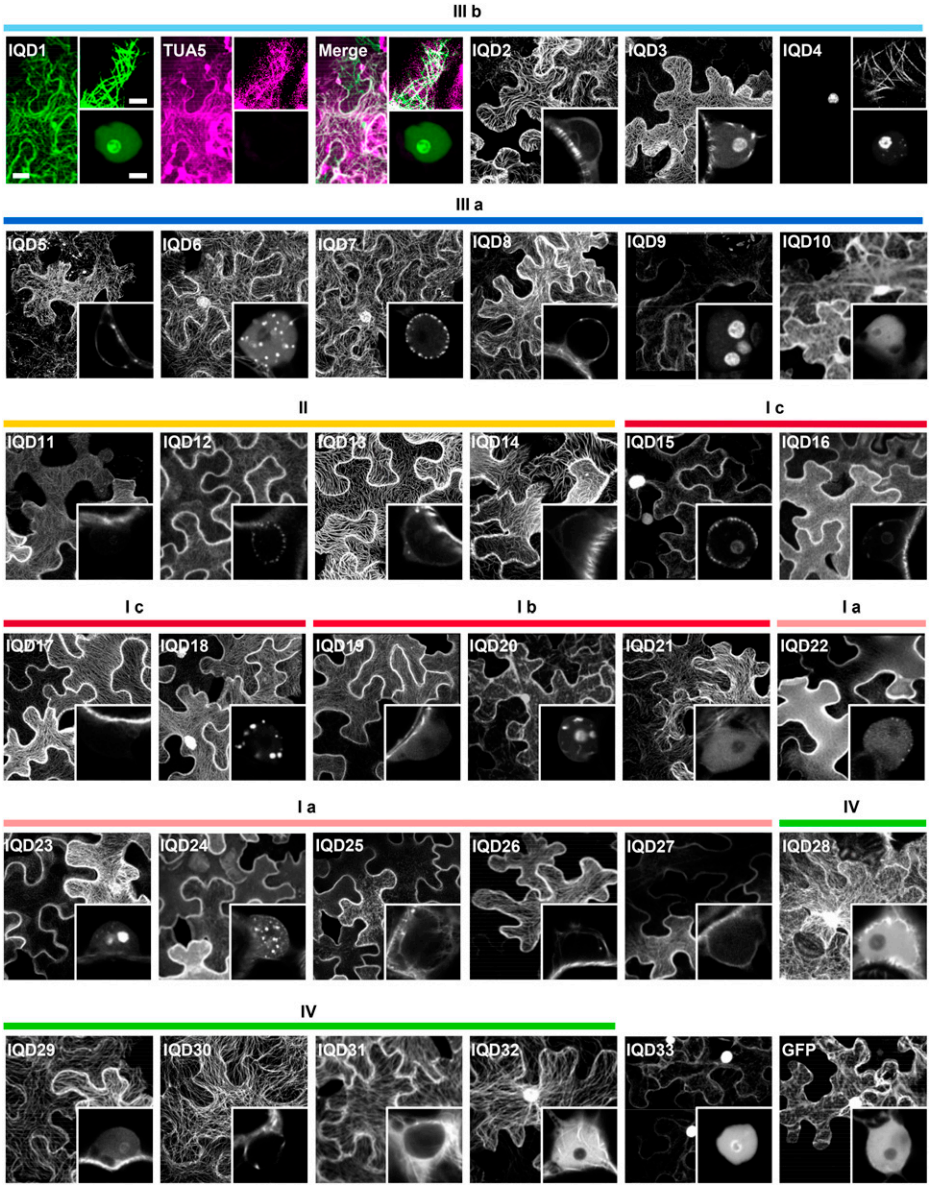

Figure 1. Subcellular localization of Arabidopsis GFP-IQD fusion proteins in *N. benthamiana*. N-terminal GFP fusions of all Arabidopsis IQD family members (IQD1–IQD33) were transiently expressed under the control of the *CaMV 35S* promoter in *N. benthamiana* leaves. Colored bars above the images indicate the phylogenetic clades (Abel et al., 2005). MT colocalization of GFP-IQDs was confirmed by coexpression with RFP-TUA5 (shown for GFP-IQD1), and GFP alone was used as a reference (bottom right image). Micrographs of cells are projections of Z-stacks; insets are single-layer images of cell nuclei. Extra insets (GFP-IQD1 and GFP-IQD4) are single-layer images of MTs, which for GFP-IQD4 reveal MT localization only with increased laser intensities. Bars = 20 μm and 5 μm (insets).

To validate the recorded subcellular localization patterns of N-terminal GFP-IQD fusion proteins, we selected six IQD members for independent localization studies, which represent the distinct localization patterns and the major phylogenetic clades of the Arabidopsis IQD family (i.e. IQD8, IQD14, IQD16, IQD20, IQD25, and IQD28; Fig. 1). We obtained similar results in the *N. benthamiana* system for the six selected C-terminal IQD-GFP fusion proteins, which we expressed under the control of either the *CaMV 35S* promoter (Fig. 2A) or the native *IQD* promoters (Fig. 2B). Transfection of Arabidopsis leaves with the corresponding *Pro-35S:GFP-IQD* constructs and analysis of subcellular GFP-IQD localization further supported the localization results (Fig. 2C). Thus, the subcellular localization of GFP-tagged IQDs is independent of GFP tag configuration, expression level, and experimental system. Expression under the control of native *IQD* promoters, however, resulted in weak fluorescence signals. In combination with in silico analyses (Toufighi et al., 2005), which indicate very low *IQD* mRNA levels (Supplemental Fig. S1C), our data suggest that *IQD* gene expression correlates with low IQD protein abundance. In conclusion, our data provide solid support for the Arabidopsis IQD family being a novel class of CaMBPs with presumed functions at MTs, at the PM, and in nuclear compartments.

A Subset of IQD Proteins Localizes to Distinct PM Subdomains

The targeting of several IQD proteins to MTs as well as to the PM prompted us to study in more detail the distribution of select IQDs displaying a prominent PM localization. Imaging of the upper surface of transiently transformed *N. benthamiana* epidermis cells revealed a nonuniform distribution of GFP-IQD proteins within the PM (Fig. 3A). IQD12 and IQD22 labeled filamentous structures that align along MTs, which is corroborated by coexpression with RFP-TUA5 (Fig. 3B). The accumulation of IQD12 and IQD22 in filamentous structures is abolished upon treatment with the MT-depolymerizing drug oryzalin (Fig. 3C). In addition, all four GFP-IQD fusion proteins mark distinct punctate structures (Fig. 3A). These patterns are reminiscent of membrane subdomains, which are largely immobile compartments within the PM (Saka et al., 2014), and thought to serve as platforms of signal transduction (e.g. during immune signaling or polarized growth; Malinsky et al., 2013; Jarsch et al., 2014). We observed similar localization patterns for two PM subdomain marker proteins of the plant-specific REMORIN (Rem) family, Rem6.6 and Rem6.7 (Jarsch et al., 2014), which we included as controls (Fig. 3A). The pattern of labeled PM domains differed and ranged from a more homogenous labeling (GFP-IQD12) to the decoration of distinct circular structures (GFP-IQD25 and GFP-Rem6.7) with an average size between ~0.11 and 0.13 μm^2 (Fig. 3, A and D). To assess the lateral stability of GFP-IQD-labeled PM domains, we performed time-lapse experiments and generated kymographs (Fig. 3, E and F). As shown for GFP-IQD25, the labeled domains remained stationary for at least 20 min (Fig. 3E, arrowheads). Similarly, PM domains labeled by the other GFP-IQD fusions were temporally stable, as indicated by continuous vertical lines in the kymographs (Fig. 3F). The high lateral stability of IQD-labeled domains together with the pattern of PM localization suggest that IQD proteins are novel components of PM subdomains in planta.

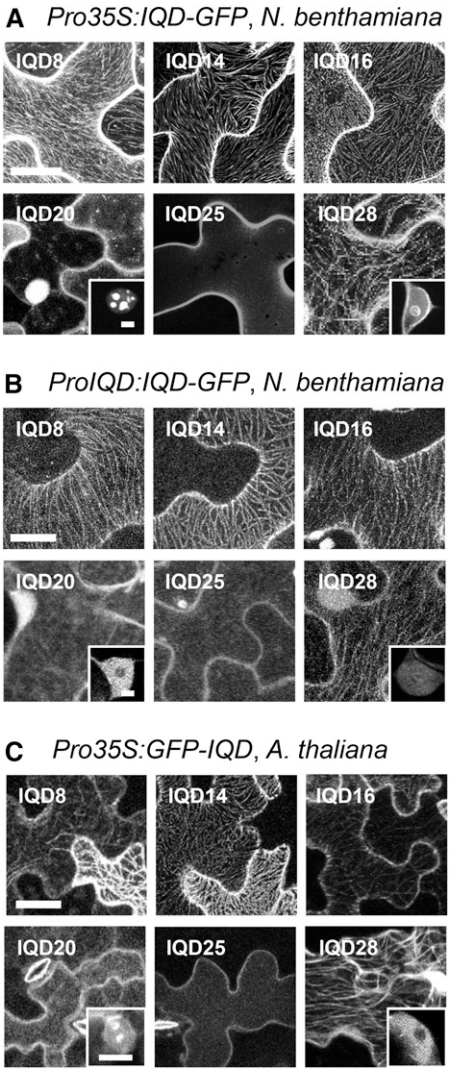

Figure 2. Independent verification of subcellular localization patterns of select Arabidopsis IQD family members. A and B, Subcellular localization of C-terminal GFP fusions of IQD proteins expressed under the control of the *CaMV 35S* promoter (A) or their endogenous regulatory elements (B) in *N. benthamiana* leaf epidermis cells. C, Subcellular localization of N-terminal GFP fusions of IQD proteins transiently expressed under the control of the *CaMV 35S* promoter in Arabidopsis leaf epidermis cells. Micrographs are projections of Z-stacks, and insets are single-layer images of nuclei. Bars = 20 μm and 5 μm (insets).

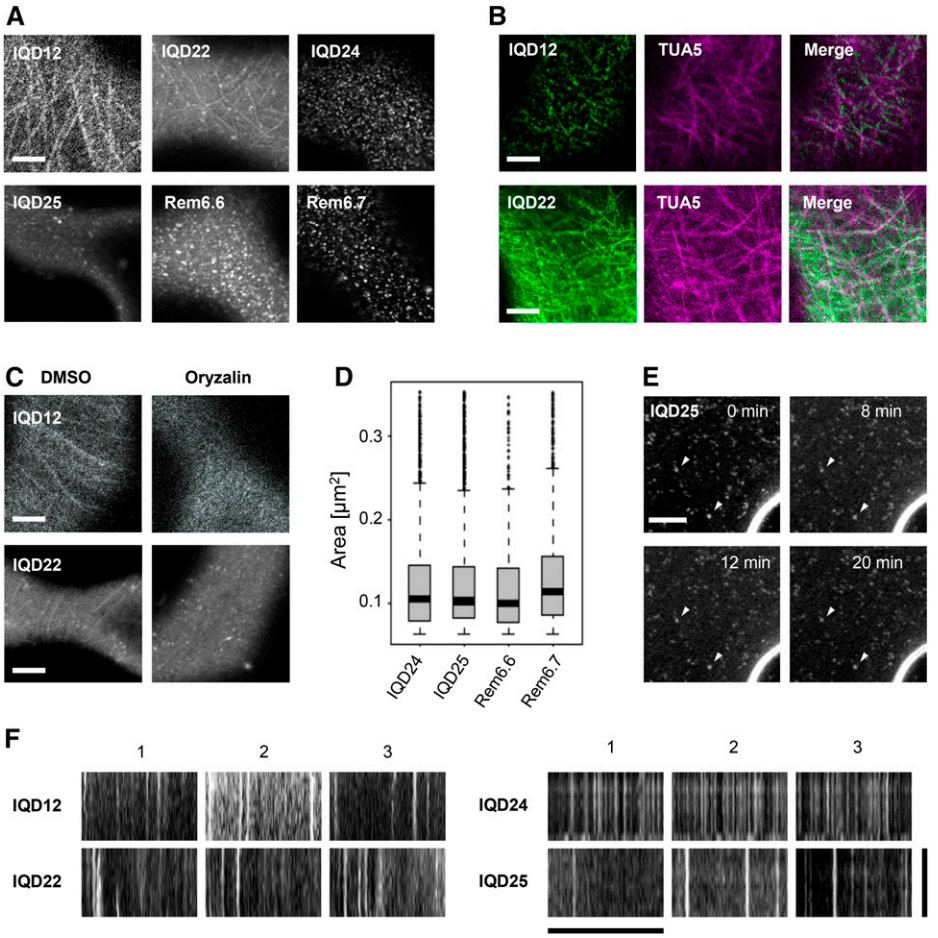

Figure 3. IQD proteins label PM subdomains in *N. benthamiana*. A, Imaging of the upper surface of *N. benthamiana* leaf epidermis cells expressing *Pro-35S*:*GFP-IQD* fusions or the PM subdomain markers *Pro-35S*:*GFP-Rem6.6* and *Pro-35S*:*GFP-Rem6.7*. B, Filamentous structures labeled by IQD12 and IQD22 aligned along MTs, as demonstrated by coexpression with RFP-TUA5. C, Depolymerization of MTs by oryzalin treatment abolishes the accumulation of IQD12 and IQD22 in filamentous structures. Bars in A to C = 5 μm. D, Quantification of domain size labeled by GFP-tagged IQD24, IQD25, Rem6.6, and Rem6.7. Data are medians of 10 independent images, and boxes range from first to third data quartiles. E, For kymographs, stacks of 10 to 14 images were acquired over 20 min in intervals of 2 min. Arrowheads indicate individual GFP-IQD25-labeled punctate structures within the PM, which remain stable over 20 min. Bar = 5 μm. F, Kymographs were created from three independent time-lapse movies (1, 2, and 3) of cells expressing GFP-tagged IQD12, IQD22, IQD24, or IQD25. Vertical lines indicate that the PM subdomains are highly immobile. Bars = 20 μm (horizontal) and 20 min (vertical).

We generated transgenic *Pro-35S*:*GFP-IQD25* lines to confirm PM localization in Arabidopsis. As observed in *N. benthamiana* leaf cells, GFP-IQD25 decorated the periphery of root cells in a punctate pattern (Fig. 4A). Our data are in agreement with work by Jarsch et al. (2014), who reported the formation of PM subdomains in *N. benthamiana* and Arabidopsis. As expected, GFP-IQD25 fluorescence colocalized upon plasmolysis with the PM and not with the cell wall, which were stained with FM4-64 and propidium iodide (PI), respectively (Fig. 4B). PM localization of GFP-IQD25 was further corroborated by immunogold labeling using an anti-GFP antibody, which indicated enrichment of gold particles at the PM in tissue sections of root apices (Fig. 4, C and D). Interestingly, the shape and size of the rosette leaves were altered in plants overexpressing GFP-IQD25 or untagged IQD25 when compared with wild-type or GFP-expressing control lines, respectively (Fig. 4E). The cotyledons of *IQD25*-overexpressing plants also showed significant alterations in the shape of epidermal pavement cells (Fig. 4, F and G). However, we did not notice visible morphological changes in *iqd25* loss-of-function lines. *ProIQD25*:*GFP-GUS* expression was detectable in the shoot apical meristem and in the youngest leaves but not in older parts of cotyledons and leaves (Supplemental Fig. S2, A–E). Thus, the observed phenotypes in *Pro-35S*:*GFP-IQD25* and *Pro-35S*:*IQD25* might be a result of ectopic expression. Alternatively, the lack of phenotypes in *iqd25* mutants possibly points to a high degree of functional redundancy within the IQD family.

Quantitative Analysis of GFP-IQD-Labeled MT Patterns

Because MT localization is a hallmark of the Arabidopsis IQD family (Fig. 1) and *IQD* overexpression alters plant development (Xiao et al., 2008; this study), we hypothesized that IQD proteins function in MT-dependent processes. To quantitatively record MT patterns, we adapted an approach used previously to measure actin structures in mammalian cells (Möller et al., 2014). We imaged epidermal cell outlines in the red channel by PI staining or by the expression of an RFP-fused PM-localized protein, PLASMODESMATA-LOCATED PROTEIN1 (PDLP1)-RFP (Amari et al., 2010), and traced GFP-IQD-decorated MT arrays in the green channel. Two-channel maximum projections of Z-stacks covering the upper half of the epidermal cell layer were analyzed, texture feature vectors were extracted from square windows based on local binary patterns (Ojala et al., 2002), and groups of MT patterns

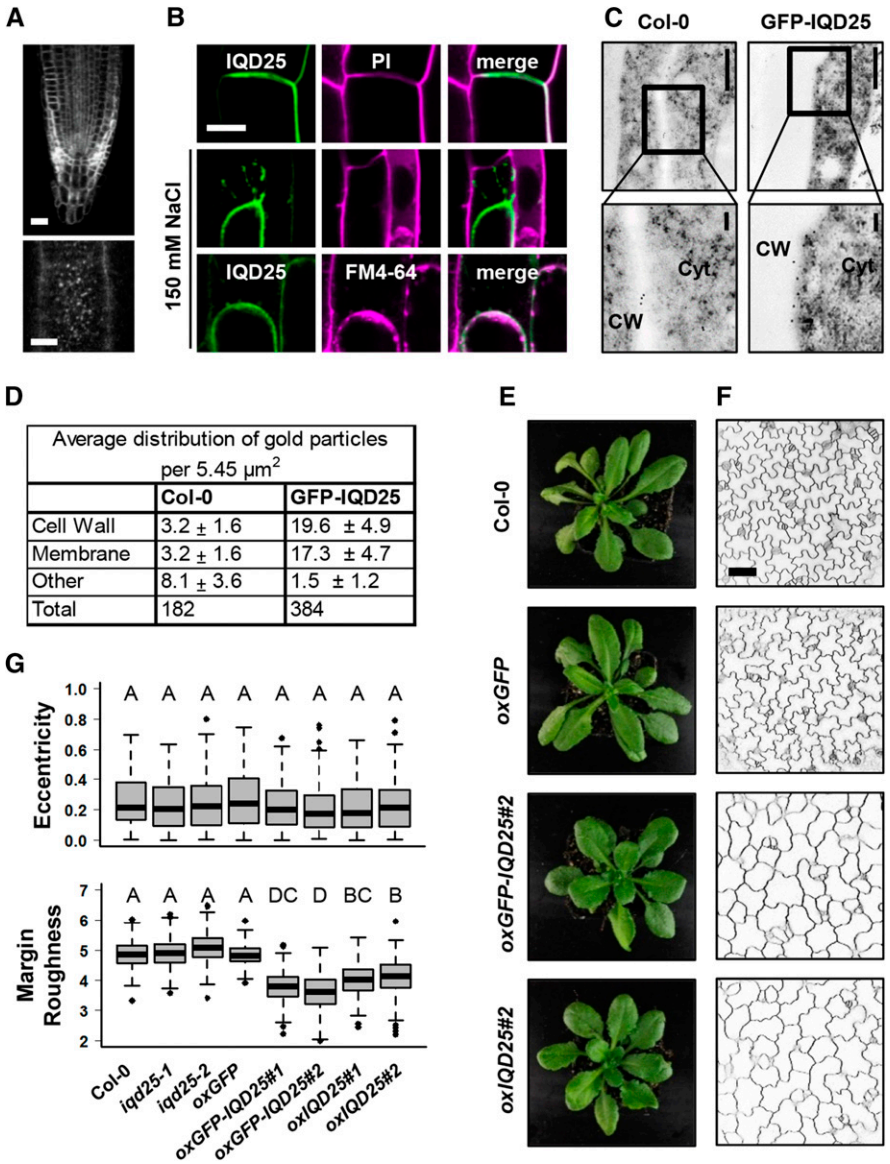

Figure 4. Subcellular localization and phenotypes in transgenic *Pro-35S:GFP-IQD25* Arabidopsis seedlings. A to C, Root cells of 4-d-old transgenic Arabidopsis seedlings expressing GFP-IQD25 under the control of the *CaMV 35S* promoter. A, Subcellular localization of GFP-IQD25 in a primary root tip (top) and surface imaging of root epidermis cells (bottom). Bars = 20 μm (top) and 5 μm (bottom). B, PM localization of GFP-IQD25. GFP-IQD25 localizes to the cell outline, as demonstrated by colocalization with the cell wall dye PI in root cells. After plasmolysis with 150 mM NaCl, GFP-IQD25 fluorescence is detached from PI-stained cell walls and colocalizes with FM4-64-stained PM. C, Localization of GFP-IQD25 by immunogold labeling and transmission electron microscopy. Bottom images are magnifications of the framed regions in the top images. CW, Cell wall; Cyt, cytosol. Bars = 0.5 μm (top) and 0.1 μm (bottom). D, Quantification of gold particles in 10 independent sections. A significant enrichment of gold particles at the PM and cell wall was observed in GFP-IQD25 when compared with the wild-type control (Columbia-0 [Col-0]). E and F, Phenotypes of wild-type, *Pro-35S:IQD25*, *Pro-35S:GFP-IQD25*, and *Pro-35S:GFP* transgenic seedlings. E, Shoots of 4-week-old plants grown on soil under long-day conditions. F, Single optical sections are shown for cotyledon epidermal cells (adaxial side) of 5-d-old seedlings grown under sterile conditions. Cell outlines were visualized with PI. Bar = 50 μm. G, Quantification of cellular elongation (eccentricity) and of the (ir)regularity/(non)smoothness of the cell contour (margin roughness). Results are medians from $n \geq 90$ cells and $n \geq 3$ seedlings, and boxes range from first to third quartiles. Different letters denote a significant statistical difference. $P < 0.005$ by one-way ANOVA.

were defined by cluster analysis (Fig. 5A). The relative distribution of windows belonging to each group was determined for each individual cell. Pairwise distances between the 23 most strongly MT-associated GFP-IQD fusions were visualized in a heat map (Fig. 5B). To validate our approach, we tested the robustness and reliability of the tool using different window sizes (16 × 16 and 32 × 32) and by applying sliding windows of sizes 8 to 32. All samples showed the same trends irrespective of the window settings. Thus, we conclude that our computational pattern-analysis tool is suitable to efficiently and robustly quantify MT array patterns. To assess MT patterns more broadly, we generated a similarity network (Fig. 5C). Our analysis revealed high similarity between MT networks labeled by IQD members of phylogenetic groups II (IQD13 and IQD14, encoded by a sister gene pair), IIIb, and IV, with the exception of IQD11 and IQD28. A second cluster includes IQD7, IQD8 (encoded by a sister gene pair), and IQD6 (the most closely related member of group IIIa; Abel et al., 2005). In general, we noticed a tendency of phylogenetically related IQDs to decorate similar MT patterns. Notably, MT patterns observed by the overexpression of GFP-tagged IQD11 and IQD16 differed from all others and potentially reflect specialized functions.

Overexpression of *IQD16* Alters MT Organization and Cell Shape

To test our pattern-analysis tool and study the functions of IQD proteins in Arabidopsis, we initially focused on IQD16 because our data indicated MT localization of

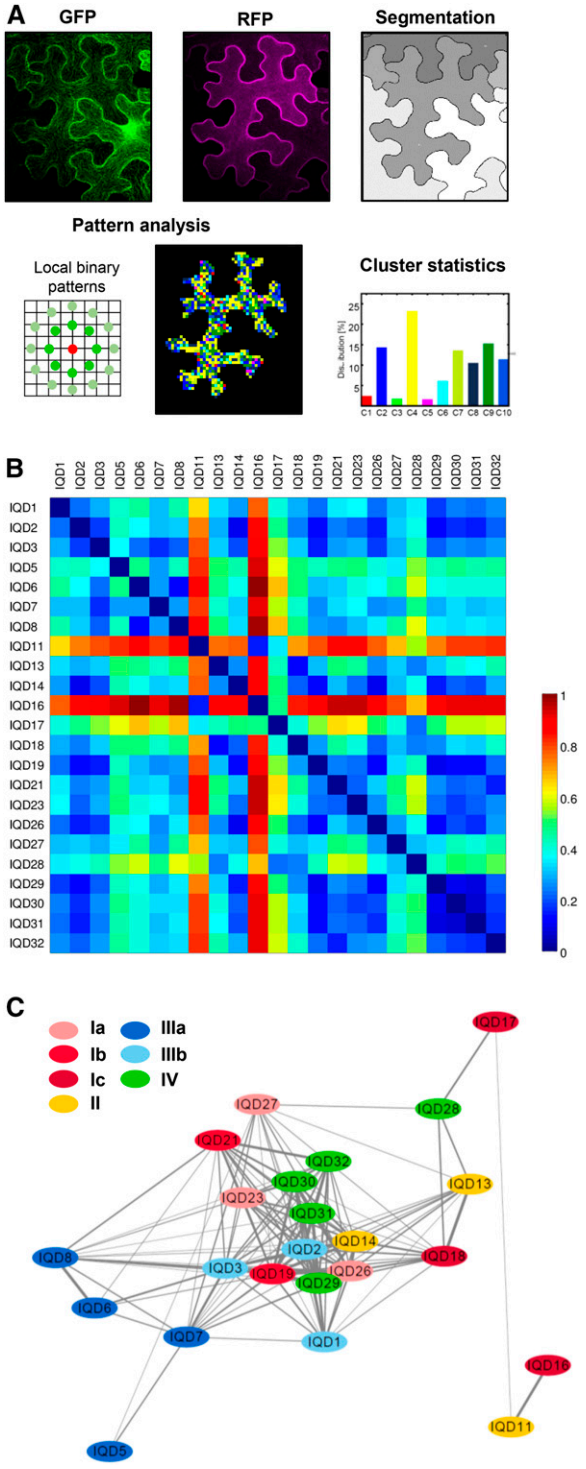

Figure 5. Quantification and network analysis of MT patterns in *N. benthamiana* epidermis cells. A, Workflow of MT pattern analysis. PI-stained cell outlines were imaged in the red channel for cell segmentation, and GFP-IQD-labeled MTs were recorded in the green channel. Texture features were extracted from local binary patterns, and groups of patterns were defined by cluster analysis. B, Heat map showing pairwise distances between MT patterns. The heat map was normalized to a range of [0,1], with blue colors representing high similarity and distances close to 0 and red colors representing high dissimilarity and distances close to 1. The color bar shown encodes the similarity strength. C, Network analysis of MT patterns induced by the overexpression of GFP-IQD fusions. Nodes represent average MT patterns of individual IQD members. Node colors highlight the phylogenetic groups and subgroups, and the width of the connecting lines is proportional to the similarity between the nodes.

IQD16 in a highly distinctive pattern (Figs. 1, 2, and 5, B and C). We did not observe phenotypic alterations for *iqd16* T-DNA loss-of-function lines, even after careful examination of tissues in which *ProIQD16:GFP-GUS* expression is detectable (Supplemental Fig. S3, A–G). However, plants overexpressing *IQD16* develop elongated aerial organs with significantly elongated cells (i.e. cotyledons, leaves, and hypocotyls) and display left-handed helical growth (Fig. 6, A–D). Phenotypic strength correlated with *Pro-35S:IQD16* expression (Fig. 6E) and suggests *IQD16* dosage-dependent effects on plant growth. *GFP-IQD16* overexpression lines display similar phenotypes (Fig. 6, A–D), indicating the functionality of the fusion protein. Helical growth aberrations and altered leaf shape were reported for tomato *sun* lines (Wu et al., 2011) and often are associated with defects in MT functions (Buschmann et al., 2004; Ishida et al., 2007). Moreover, the growth defects are reminiscent of plants overexpressing *LONGIFOLIA1/TON1 RECRUITING MOTIF2* (*TRM2*), which encodes a plant-specific MAP (Lee et al., 2006; Drevensek et al., 2012). Hence, the observed phenotypes point to roles of IQD16 in the regulation of MT arrays.

To analyze MT organization, we crossed the *GFP-MAP4* marker (Marc et al., 1998) into *Pro-35S:IQD16* lines. When compared with the parental wild-type (*GFP-MAP4*) line, light-grown plants overexpressing *IQD16* (*GFP-MAP4*) or *GFP-IQD16* displayed significantly elongated cells (Fig. 6, F and G), and the increased cell length of *IQD16* overexpression plants correlated with an altered orientation of cortical MTs (Fig. 6, H and I). Consistent with previous reports (Hamada et al., 2013), MTs in wild-type (*GFP-MAP4*) hypocotyl cells were distributed randomly. However, in *IQD16* (*GFP-MAP4*) and *GFP-IQD16*-overexpressing lines, MTs decorated by the GFP reporter were aligned preferentially in oblique arrays with angles between 40° and 70° (Fig. 6I). Thus, our experiments show that IQD16 localizes to cortical MTs in Arabidopsis and impacts MT orientation and cell shape.

Overexpression of *IQD11* and *IQD14* Differentially Modulates Plant Growth

We extended our analysis in Arabidopsis to validate the roles of additional IQD proteins at MTs (Fig. 7). We selected IQD11, which labeled MT patterns highly similar to IQD16 in the *N. benthamiana* system (Fig. 5), and IQD14, which decorates MT arrays in *N. benthamiana* (Fig. 1) and Arabidopsis (Fig. 2) in patterns different from IQD11 and IQD16 (Fig. 5). Consistent with the high similarity of MT patterns upon

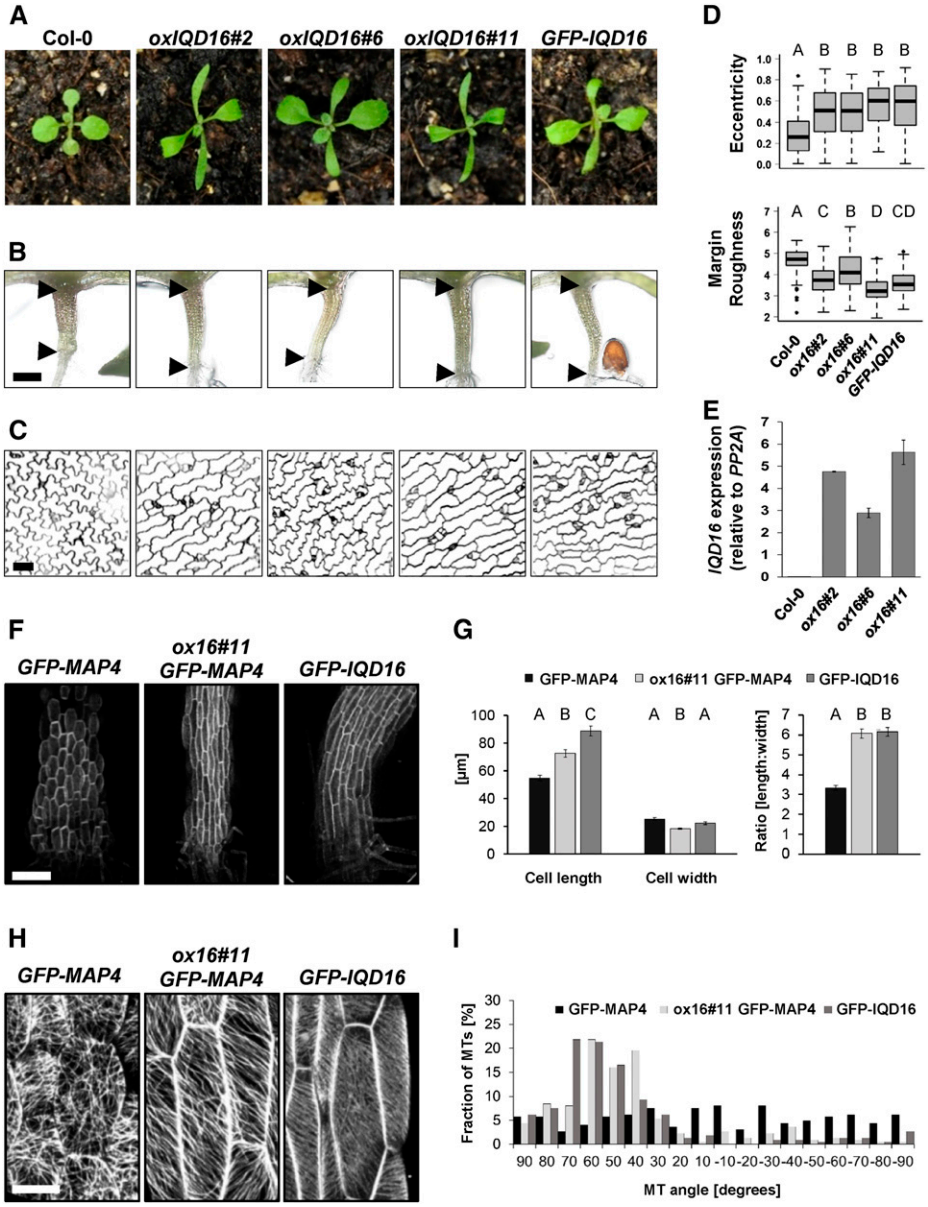

Figure 6. *IQD16* overexpression alters epidermal cell shape and cortical MT orientation. A to C, Phenotypes of Arabidopsis wild-type plants and *IQD16*-overexpressing plants grown under long-day conditions. Shown are representative images of shoots of the wild type (Col-0), three independent transgenic *Pro-35S:IQD16* lines (*ox16#2*, *ox16#6*, and *ox16#11*), and one transgenic *Pro-35S:GFP-IQD16* line (*GFP-IQD16*). A, Two-week-old plants grown on soil. B, Seven-day-old seedlings grown under sterile conditions. Arrowheads delimit hypocotyls, which are elongated in *IQD16*-overexpressing plants. Bar = 0.5 mm. C, Single optical sections of adaxial epidermal pavement cells in cotyledons of 5-d-old seedlings. Cell walls were visualized with PI. Bar = 50 μm. D, Quantification of the cellular eccentricity and margin roughness in cells shown in C. Results are medians from $n \geq 70$ cells and $n \geq 3$ seedlings, and boxes range from first to third quartiles. Different letters denote a significant statistical difference. $P < 0.005$ by one-way ANOVA. E, Quantitative reverse transcription (RT)-PCR analysis of *IQD16* transcript levels relative to *PP2A* in the three individual *Pro-35S:IQD16* transgenic lines shown in A in comparison with the wild type (Col-0). Results are averages of three replicates ± SE. F and G, Analysis of MT organization and cell shape in transgenic seedlings expressing *Pro-35S:GFP-MAP4* (*GFP-MAP4*), *Pro-35S:IQD16* and *Pro-35S:GFP-MAP4* (*oxIQD16#11 GFP-MAP4*), or *Pro-35S:GFP-IQD16* (*GFP-IQD16*). Seedlings of stably transformed Arabidopsis lines (5 d old) were grown on Arabidopsis salt medium under long-day conditions. F, Z-stack projections of hypocotyl epidermis cells. Bar = 100 μm. G, Epidermal hypocotyl cell size. Cell length and cell width were measured relative to the perpendicular axis, and the length-to-width ratio of individual cells was calculated (means ± SE, n = 33 cells of three seedlings; Different letters denote a significant statistical difference. $P < 0.005$ by Student's t test). H, Z-stack projections of individual epidermal hypocotyl cells. Bar = 20 μm. I, Quantification of cortical MT orientation. Angles were measured relative to the perpendicular axis, and relative fractions were calculated (n = 225 MTs, with three independent experiments).

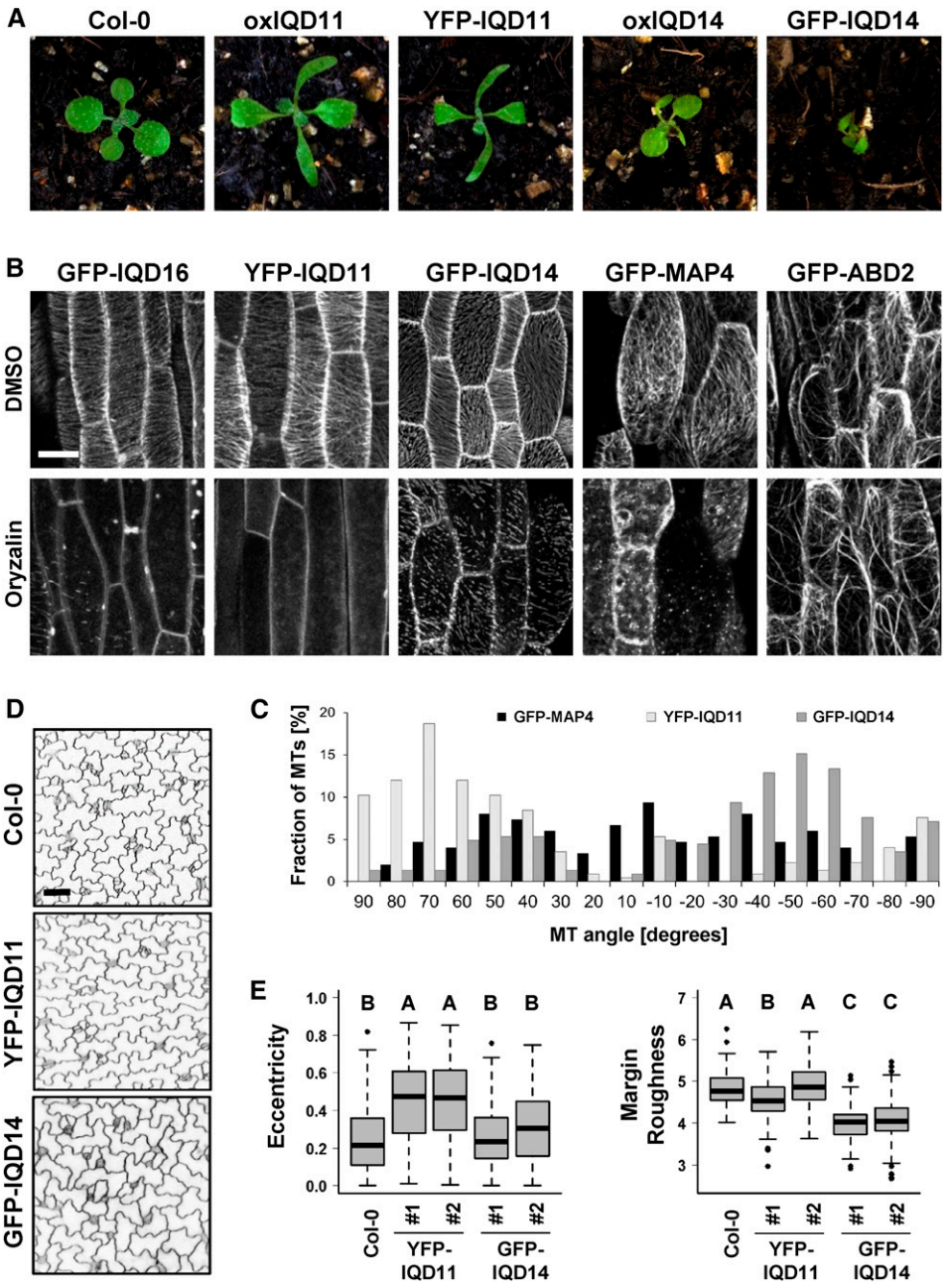

Figure 7. *IQD11* and *IQD14* overexpression lines display altered plant growth and MT orientation. A, Phenotypes of Arabidopsis wild-type and transgenic plants overexpressing *IQD11* and *IQD14*. Shown are representative images of shoots of 2-week-old plants grown under long-day conditions from the wild type (Col-0) and transgenic *Pro-35S:IQD11* (oxIQD11), *Pro-35S:YFP-IQD11* (YFP-IQD11), *Pro-35S:IQD14* (oxIQD14), and *Pro-35S:GFP-IQD14* (GFP-IQD14) lines. B, Subcellular localization of GFP-IQD16, YFP-IQD11, GFP-IQD14, GFP-MAP4, and GFP-ABD2 fusion proteins in seedlings treated with dimethyl sulfoxide (DMSO) or with the MT-depolymerizing drug oryzalin. Seedlings of transgenic Arabidopsis lines (5 d) were grown on Arabidopsis salt medium under long-day conditions. Micrographs are Z-stack projections of epidermal hypocotyl cells. Bar = 20 μm. C, Quantification of cortical MT orientation (Fig. 6). D, Epidermal pavement cell shape in the wild type and in transgenic *Pro-35S:YFP-IQD11* and *Pro-35S:GFP-IQD14* lines. Single optical sections show adaxial epidermal pavement cells in cotyledons from 5-d-old seedlings. Cell walls were visualized with PI. Bar = 50 μm. E, Quantification of the cellular eccentricity and margin roughness in cells. Results are medians from $n \geq 90$ cells and $n \geq 4$ seedlings, and boxes range from first to third quartiles. Different letters denote a significant statistical difference. $P < 0.001$ by one-way ANOVA.

overexpression of *GFP-IQD16* and yellow fluorescent protein (YFP)-IQD11 in *N. benthamiana* (Fig. 5), the phenotypes of transgenic Arabidopsis plants overexpressing *IQD11* or *YFP-IQD11* resembled those of *IQD16* overexpression lines (Figs. 6 and 7A; Supplemental Fig. S4). YFP-IQD11 labeled MT arrays in patterns similar to GFP-IQD16 in epidermal hypocotyl cells of transgenic Arabidopsis seedlings (Fig. 7, B and C), and overexpression of YFP-IQD11 induced the elongation of epidermis pavement cells (Fig. 7, D and E). We observed distinct phenotypes upon overexpression (*Pro-35S*) of *IQD14* or *GFP-IQD14* (Fig. 7A; Supplemental Fig. S4A). Transgenic plants displayed strongly induced organ twisting but no changes in leaf elongation (Fig. 7, A, D, and E). Similar phenotypes were reported for *tortifolia* and *spiral* mutants (Furutani et al., 2000; Buschmann et al., 2004; Shoji et al., 2004). Helical growth defects commonly correlate with an increased transverse alignment of MTs (Ishida et al., 2007), which are visible upon the overexpression of YFP-IQD11, GFP-IQD14, and GFP-IQD16 (Figs. 6I and 7C). We confirmed the MT specificity of GFP-IQD16, YFP-IQD11, and GFP-IQD14 by the treatment of transgenic Arabidopsis seedlings with the MT-depolymerizing drug oryzalin (Fig. 7B, bottom row). We included transgenic GFP-MAP4 (Marc et al., 1998) and GFP-ABD2 (Sheahan et al., 2004; Wang et al., 2004) lines as controls for the MT and actin cytoskeleton, respectively. Oryzalin

treatment efficiently disrupted MT networks but had no effect on the actin cytoskeleton. Analysis of *ProIQD11*:*GFP-GUS* and *ProIQD14*:*GFP-GUS* expression revealed *IQD11* and *IQD14* promoter activity in the hypocotyl, cotyledons, leaf tissues, and petioles (Supplemental Fig. S4B). Thus, the phenotypes in combination with the observed MT localization suggest that elevated levels of IQD proteins may have diverse effects on MT organization and cell growth control in tissues with endogenous *IQD* expression. Moreover, our pattern-analysis tool proves to be a useful resource for the study of MT organization in complex shaped cells and provides, to our knowledge, the first experimental evidence for roles of IQD proteins in the regulation of MT networks and cell shape.

IQD Family Members Differentially Recruit CaM to Diverse Subcellular Sites

The differential subcellular localization of IQD family members (Fig. 1) prompted us to test whether IQD proteins recruit CaM to diverse subcellular sites. We selected eight IQD proteins representing the phylogenetic clades and different localization patterns of the Arabidopsis IQD family and performed bimolecular fluorescence complementation (BiFC) assays, which detect protein-protein interactions in planta with subcellular resolution (Gehl et al., 2009; Kudla and Bock, 2016). Coexpression in *N. benthamiana* of nYFP-IQD1 and cYFP-CaM2 reconstitutes YFP fluorescence at MTs and in the nucle(ol)us (Fig. 8), which is highly similar to the observed GFP-IQD1 localization (Fig. 1). Similarly, cYFP-CaM2 interacted with nYFP fusions of IQD8, IQD13, IQD16, and IQD32 at MTs. For nYFP-IQD20 and nYFP-IQD25, BiFC signals were detected in distinct PM subdomains, and nYFP-IQD33 interacted with cYFP-CaM2 in the nucleus (Fig. 8, insets). nYFP-TRM1 (Drevensek et al., 2012) served as a negative control, and the recovery of YFP fluorescence was not detectable with cYFP-CaM2, which confirmed the specificity of the BiFC assay. We independently verified the physical in vivo interactions of CaM2 and select IQDs by coexpression studies, which revealed GFP-IQD fusion protein-dependent relocalization of RFP-CaM2 (Supplemental Fig. S5). When coexpressed with GFP alone, RFP-CaM2 accumulated in the cytosol and nucleus, whereas coexpression with GFP-IQD1 induced the recruitment of RFP-CaM2 to MTs and the nucleolus, as reported previously (Bürstenbinder et al., 2013). In addition, coexpression with GFP-IQD8, GFP-IQD13, GFP-IQD16, or GFP-IQD32 caused the recruitment of RFP-CaM2 to MTs, and relocalization of RFP-CaM2 to the PM was evident upon coexpression with GFP-IQD25. Thus, IQD proteins recruit CaM2 and possibly other CaM/CMLs to MTs, PM subdomains, and nuclear compartments. Interaction of IQD proteins with CaM2 did not abolish IQD localization to MTs or the PM, suggesting that subcellular targeting of IQD proteins is independent of CaM recruitment.

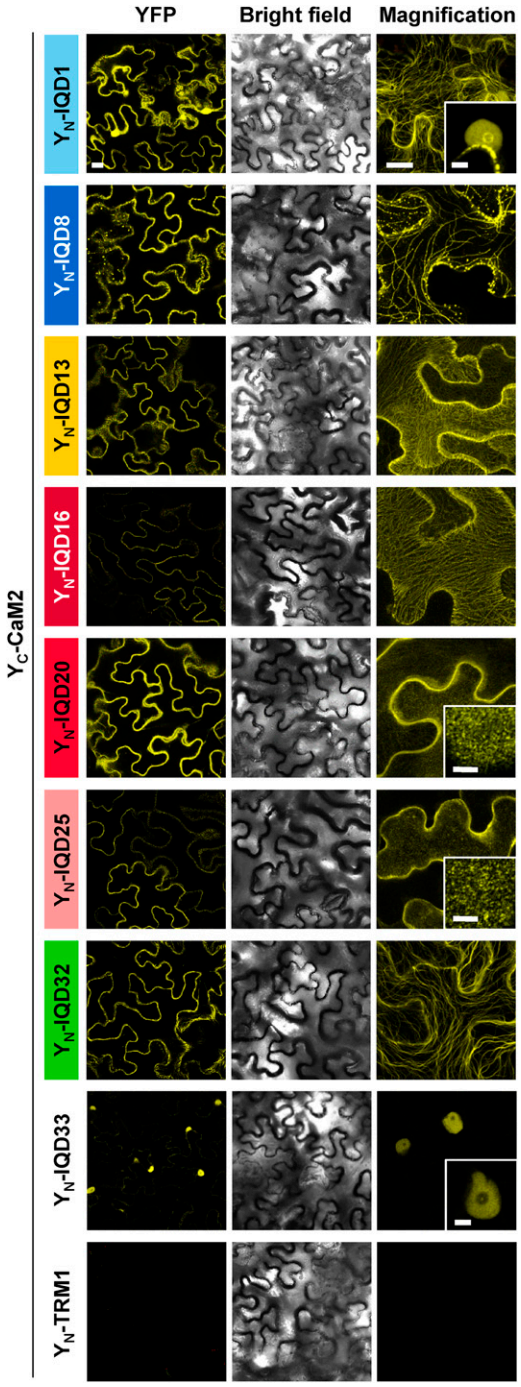

Figure 8. IQD proteins interact with CaM2 at MTs, at the PM, and in the nucleus. Single optical sections of BiFC signals (left column) and corresponding bright-field images (center column) as well as closeup Z-stack images of YFP fluorescence (right column) are shown for *N. benthamiana* epidermis cells after coexpression of IQD proteins N-terminally tagged with the N-terminal half of Venus (Y_N) and CaM2 N-terminally tagged with the C-terminal half of Venus (Y_C). Insets in the right column show nuclei or the membrane surface. Y_N-TRM1 was used as a negative control. Bars = 50 μm (left column), 20 μm (right column), and 5 μm (insets).

DISCUSSION

Plants evolved a remarkable repertoire of proteins for decoding information encrypted by cellular Ca^{2+} signatures, which are transiently generated in specific responses to numerous systemic or environmental stimuli. CaM/CML polypeptides are principal Ca^{2+} sensor relays that control the biochemical activities of diverse regulatory targets via complex Ca^{2+}-dependent and Ca^{2+}-independent interactions (Dodd et al., 2010; Kudla et al., 2010; Hashimoto and Kudla, 2011). Knowledge of the CaM/CML targets and of their biochemical functions and underlying biological processes will be imperative for deciphering CaM-mediated Ca^{2+} signal transduction in plants (Yang and Poovaiah, 2003). Plant-specific *IQD* gene families, first annotated in Arabidopsis and rice (Abel et al., 2005) and more recently in five additional species (Filiz et al., 2013; Huang et al., 2013; Feng et al., 2014; Ma et al., 2014; Wu et al., 2016), possibly encode the largest class of CaMBPs in plants. Although the roles of a few IQD members are beginning to emerge, the precise molecular functions and mechanisms of action are still elusive for any IQD protein (Abel et al., 2013).

We previously identified Arabidopsis IQD1 in a genetic screen for glucosinolate-related mutants (Levy et al., 2005) and noticed its colocalization with cortical MT arrays (Bürstenbinder et al., 2013). In this study, we report the subcellular distribution patterns of all 33 Arabidopsis IQD family members in transiently transfected *N. benthamiana* cells, which revealed that most GFP-IQD fusion proteins differentially localize to the PM, to the cortical MT network, and to distinctive sites of the cell nucleus (Fig. 1). We confirmed the localization patterns of select IQD proteins (Fig. 2), which were independent of GFP tag configuration (N or C terminal), promoter strength (*Pro-35S* and *ProIQD*), and expression system (*N. benthamiana* and Arabidopsis). The localization of GFP-fused IQD proteins to MT arrays, the PM, and the cell nucleus is in agreement with published proteome data. Analysis of MAP-enriched fractions prepared from Arabidopsis cell cultures identified a large set of known and novel MAPs. Interestingly, four IQD proteins of phylogenetic group IV (IQD28, IQD29, IQD31, and IQD32) were highly enriched in these fractions, and MT colocalization was confirmed for GFP fusions of IQD28 and IQD32 (Hamada et al., 2013). A phosphoproteome analysis of PM-associated proteins after elicitor treatment identified several IQDs in PM-enriched fractions, including IQD9, IQD11, and IQD14 (Benschop et al., 2007). Interrogation of the nuclear proteome detected IQD28 (Bigeard et al., 2014; Palm et al., 2016) and IQD32 (Bigeard et al., 2014), which independently confirms the targeting of at least two IQD proteins to multiple subcellular sites (Hamada et al., 2013).

While our work provides evidence for the nuclear, MT, and PM localization of most IQD family members, we are left to speculate about the modes of subcellular IQD targeting. In several MAPs, the binding to MTs is mediated by positively charged motifs, most likely via electrostatic interaction with acidic tail motifs of tubulin subunits (Smith et al., 2001; Mishima et al., 2007; Drevensek et al., 2012; Roll-Mecak, 2015). Similarly, membrane-binding motifs used to anchor proteins to the acidic phospholipid surface of membranes often consist of basic amino acids (Goldenberg and Steinberg, 2010; Scott et al., 2013), and nuclear localization signals require core basic residues for their activity (Kosugi et al., 2009). The high basic pI of IQD proteins (~10.3), which is a hallmark of the family (Abel et al., 2005), suggests that electrostatic interaction contributes to the MT and PM attachment of IQD proteins, and charge-plot analysis reveals the occurrence of basic patches in all 33 Arabidopsis IQD members (Supplemental Fig. S6). Membrane tethering of IQD proteins is possibly stabilized by *S*-acylation (or palmitoylation), which attaches fatty acids to internal Cys residues. In silico analyses using the GPS-Lipid and CSS-Palm tools (Ren et al., 2008; Xie et al., 2016) predicted the presence of *S*-acylation sites in several IQD family members (Supplemental Table S1). Experimental support for the lipidation of IQD proteins is provided by a large-scale proteomics data set, which reported *S*-acylation of IQD32 (Hemsley et al., 2013).

The four PM-localized GFP-IQD fusions that we examined in more detail (IQD12, IQD22, IQD24, and IQD25) labeled distinct and immobile PM subdomains, which suggests specific cellular functions for each IQD (Fig. 3). Studies in *Saccharomyces cerevisiae* (yeast) and Arabidopsis revealed that different populations of subdomains coexist in membranes (Spira et al., 2012; Jarsch et al., 2014). Notably, *S*-acylation appears to play a predominant role for protein anchoring at membrane subdomains in plants (Hemsley and Grierson, 2008), as has been demonstrated for Rho-like GTPases (Craddock et al., 2013) and for plant-specific scaffold proteins of the Rem family (Konrad et al., 2014; Konrad and Ott, 2015). Individual subdomains are thought to reflect specialized functions of PM-associated protein complexes, such as in signal transduction (Malinsky et al., 2013), because protein components of functional modules tend to colocalize in the same type of membrane subdomains. Such copartitioning was reported recently for the brassinosteroid receptor BRASSINOSTEROID INSENSITIVE 1 (BRI1) and the subdomain marker ARABIDOPSIS FLOTILLIN-LIKE PROTEIN 1 (AtFlot1) (Wang et al., 2015) as well as for the anion channel SLAC1-HOMOLOGUE 3 (SLAH3) and the Ca^{2+}-dependent protein kinase CPK21 (Demir et al., 2013). IQD-dependent recruitment of CaM to membrane subdomains (Fig. 7) is particularly intriguing, as it may locally restrict CaM-mediated Ca^{2+} signaling to specific sites within the PM and to spatially separate functionally distinct CaM signaling modules. Thus, the identification of IQD-interacting proteins within individual PM subdomains will be key for elucidating modules of CaM signaling pathways and assigning functions to individual IQD family members.

Lateral stability is a hallmark of membrane subdomains, and their stabilization within the PM requires scaffolding functions of the cytoskeleton (Kusumi et al., 2012). Colocalization with RFP-TUA5 revealed that the PM subdomains labeled by GFP-tagged IQD proteins partially align along MT arrays (Fig. 3). Similar patterns have been reported for Rem proteins (Raffaele et al., 2007; Jarsch et al., 2014), and targeting of AtRem6.6 to subdomains in the PM proved to be sensitive to MT-depolymerizing drugs (Jarsch et al., 2014), as was the case for IQD12 and IQD22 (Fig. 3). A function of the PM-MT nexus for subdomain formation is further supported by studies in yeast also in S. cerevisiae (Kusumi et al., 2012). In addition, the plant PM-MT interface plays important roles in cell wall biogenesis and cell shape regulation, mainly by guiding the deposition of nascent cellulose fibers. Cellulose biosynthesis requires the delivery of CSCs to the PM and the coordination of CSC trajectories along MT arrays (Liu et al., 2015). The dual localization of several IQD proteins to MTs and the PM, and the cell shape defects caused by *IQD* overexpression (Figs. 5–7), are consistent with a function of IQDs at the PM-MT connection. A striking transverse alignment of cortical MTs, as observed for *IQD*-overexpressing cells (Figs. 6 and 7), often correlates with a spiral pattern of cellulose deposition, which favors longitudinal cell expansion (Ivakov and Persson, 2013). Despite decades of research, it is not well understood how CSCs interact with MTs and how MTs are tethered to the PM. Our study identified IQD family members as putative candidates mediating such interactions. Elucidating how IQD proteins contribute to functional PM-MT connections (e.g. by affecting cellulose deposition, subdomain formation, or MT attachment to the PM) will be a challenging task for the future.

The differential effects of overexpressed IQD family members on MT arrays and the MT-related phenotypes of *IQD*-overexpressing Arabidopsis plants point to roles of IQDs in the organization of MT networks. Interestingly, we noticed that most GFP-IQD proteins uniformly decorated MT arrays, similar to members of the MAP65 family (Lucas et al., 2011), which function mainly in MT bundling (Chen et al., 2016). In contrast, most other MAPs either accumulate at the plus end of MTs, such as CLIP-ASSOCIATED PROTEIN (CLASP) (Kirik et al., 2007), END BINDING PROTEIN EB1 (Bisgrove et al., 2008), or SPIRAL1 (SPR1) (Sedbrook et al., 2004), where they regulate the dynamics of MT growth and shrinkage, or associate in punctate to patchy patterns preferably at newly formed MT crossover sites, as described for KATANIN 1(KTN1) (Lindeboom et al., 2013) and SPR2 (Shoji et al., 2004). Evenly distributed MT association suggests that IQD proteins may influence MT bundling. However, further work is required to uncover the mechanisms by which IQDs modulate MT organization. In vivo studies on IQD dynamics and cellular functions have been hampered by low levels of IQD protein abundance and a high degree of genetic redundancy within the IQD family. Therefore, transient expression assays combined with our computational tool to quantitatively analyze MT patterns may prove beneficial for elucidating IQD functions. By applying this tool in a proof-of-concept study, we identified IQD16 and IQD11 as the most divergent IQD members in terms of MT patterning (Fig. 5) and confirmed their function in regulating MT orientation and cell shape in transgenic Arabidopsis plants (Figs. 6 and 7). Differential MT-modulating functions of individual IQDs are further corroborated by MT-related phenotypes in *IQD14*-overexpressing Arabidopsis seedlings (Fig. 7). Therefore, we conclude that MT arrays are sensitive to reorganization by (transient) overexpression of *IQDs*. Comparison of MT patterns caused by the overexpression of IQDs with the MT patterns formed upon the overexpression of MAPs with known functions (e.g. in bundling or cross-linking of MTs) could assist to predict molecular mechanisms of IQD functions. Thus, transient expression assays combined with our computational tool of MT array pattern analysis offers a useful resource with which to study potential regulators of MT organization in complex shaped cells. Functions in growth regulation, however, are not limited to MT-localized IQD family members, as revealed by altered cell shapes in plants overexpressing the PM-localized IQD25. Notably, we observed distinct and, in some cases, even opposing effects on growth and cell shape formation for the analyzed IQD members (i.e. increased/augmented/more pronounced elongation of leaves and cells in *IQD11*- and *IQD16*-overexpressing plants and rounding/more compact leaves and cells in *IQD25*-overexpressing plants; Figs. 4, 6, and 7). These results suggest specialized functions of individual IQDs in regulating the direction of cell elongation and possibly in cell polarity establishment.

We demonstrated in BiFC assays that select IQD members recruit CaM2 to diverse subcellular sites, which was confirmed independently by the relocalization of cytoplasmic CaM2 upon coexpression with each IQD protein (Fig. 8; Supplemental Fig. S5). Although we tested only one CaM isoform versus eight IQD proteins, it is likely that all IQD family members interact with a select set of the four CaM and 50 CML Ca^{2+} sensor polypeptides in Arabidopsis. We previously verified the predicted function of the conserved IQ67 domain for CaM binding and demonstrated in yeast two-hybrid assays the interaction of IQD1 with three CaM isoforms and of IQD20 with CaM2 and CML13 (Bürstenbinder et al., 2013). We are left to speculate on the Ca^{2+} state of recruited CaM because the IQ67 domain contains multiple Ca^{2+}-dependent and Ca^{2+}-independent CaM retention motifs and IQD20 binds in vitro to both apo-CaM and Ca^{2+}-CaM (Abel et al., 2005). The biochemical properties and functions of IQD proteins may be regulated directly upon binding to CaM and determined by its Ca^{2+} occupancy. Stimulus-specific activation of Ca^{2+} signaling pathways may specify and fine-tune the IQD affinity to MTs, the PM, and other interactors, such as IQD1-binding

KLCR1 (Bürstenbinder et al., 2013). Alternatively, as reported for fungal and mammalian IQGAP scaffold proteins, which orchestrate cellular signaling from the PM to the nucleus (Shannon, 2012; Smith et al., 2015), IQDs may act as reservoirs for CaM/CMLs. In that case, IQD proteins sequester apo-CaM/CMLs at specific subcellular sites, which upon Ca^{2+} sensing and loading are transferred to targets regulated by holo-CaM/CMLs, or vice versa. Thus, the IQD family may provide an assortment of versatile platform proteins that facilitate and specify CaM/CML dynamics during Ca^{2+} signaling at the cell periphery, on the cytoskeleton, and in the cell nucleus. Interactions of IQDs and CaM/CMLs in the nucleus may integrate nuclear calcium signaling (Charpentier and Oldroyd, 2013) and regulate a proposed function of select IQD proteins during mRNA maturation, export, and cytoplasmic transport (Abel et al., 2013; Bürstenbinder et al., 2013). These processes share nucleocytoplasmic protein factors and allow for efficient fine-tuning of protein targeting and activity (Marchand et al., 2012; Shahbabian and Chartrand, 2012).

Several properties of IQD family members point to their roles as scaffold or adaptor proteins. The central conserved IQ67 domain of most IQD proteins, which likely adopts an α-helical fold, is flanked on either side by extensive regions of predicted intrinsic disorder (Supplemental Fig. S6). Substantial intrinsic disorder is a hallmark of scaffolding proteins. The conformational flexibility and biochemical properties of natively unstructured regions, which often contain multiple, short linear peptide motifs for molecular interactions and/or posttranslational modifications (Tompa et al., 2014), specify and fine-tune the assembly of macromolecular complexes via induced and cooperative folding (Babu et al., 2011; Wright and Dyson, 2015). Because intrinsically disordered proteins are prone to engage in promiscuous molecular interactions via peptide motifs of low complexity, their steady-state concentrations are tightly regulated at multiple levels, and elevated gene expression often causes detrimental effects or disease (Vavouri et al., 2009; Babu et al., 2011). While almost nothing is known about the control of *IQD* gene expression and IQD protein stability, with the exception of *IQD22*, which is induced rapidly by GA_3 via DELLA-dependent regulation (Zentella et al., 2007), it is of note that IQD-related phenotypes have been reported only for *IQD*-overexpressing plants, which display altered secondary metabolism (Levy et al., 2005), cell shape (Figs. 6 and 7), and organ morphology (Xiao et al., 2008).

In conclusion, our comprehensive study of subcellular localization patterns of all 33 Arabidopsis IQD proteins, in combination with the computational analysis of MT arrays, in planta CaM interaction assays of select IQD members, and characterization of *IQD11*, *IQD14*, *IQD16*, and *IQD25* overexpression lines, provide strong evidence that plant-specific IQD families define a new class of largely MT-based CaMBPs with additional but distinctive roles in PM subdomains and nuclear compartments. We propose that IQD families provide a multifaceted toolbox of scaffold-like proteins for integrating CaM-dependent Ca^{2+} signaling and possibly other signal transduction pathways at multiple subcellular sites to regulate cell function, shape, and growth during plant development.

MATERIALS AND METHODS

Plant Materials and Growth Conditions

Nicotiana benthamiana plants were grown in a greenhouse at 22°C to 24°C under long-day conditions (16 h of light/8 h of dark). Arabidopsis (*Arabidopsis thaliana*) ecotype Col-0 seeds were originally obtained from the Arabidopsis Biological Resource Center. Seeds of *iqd16-2* (SALK_053223), *iqd25-1* (SALK_058876), and *iqd25-2* (SALK_148613) T-DNA lines were obtained from the Nottingham Arabidopsis Stock Centre (Scholl et al., 2000). To visualize MT arrays, transgenic Arabidopsis seedlings expressing a GFP fusion of the MT-binding domain of mouse MAP4 under the control of the *CaMV 35S* promoter were analyzed (Marc et al., 1998). For growth under semicontrolled conditions, plants were stratified at 4°C for 2 d and cultivated under long-day conditions as described above. For sterile cultivation, Arabidopsis seeds were surface sterilized with chlorine gas and, after 2 d of stratification, grown vertically on square plates containing Arabidopsis salt medium and 1% (w/v) agar with cycles of 16 h of light and 8 h of dark (Lincoln et al., 1990).

Plasmid Construction

DNA sequence information of *IQDs*, *PDLP1*, *TRM1*, *Rem6.6*, *Rem6.7*, and *TUA5* was obtained from The Arabidopsis Information Resource. Open reading frames were amplified from the Arabidopsis Biological Resource Center or RIKEN cDNA clones or from cDNA of Arabidopsis Col-0 seedlings using gene-specific primers (Supplemental Tables S2 and Table S4). Full-length genomic loci and upstream promoter sequences were amplified from genomic DNA of Arabidopsis Col-0. Amplicons were ligated into Gateway-compatible entry or donor vectors (Supplemental Table S2), and insert fidelity was verified by DNA sequencing. The generation of CaM2 ENTR plasmid was described by Fischer et al. (2013). Inserted sequences were mobilized into pB7WGF2, pB7WGY2 (Karimi et al., 2002), or pGWB455 (Nakagawa et al., 2007) for the expression of the N-terminal GFP, YFP, or RFP fusion under the control of the *CaMV* 35S promoter, respectively, or into pB7FWG or pB7FWG2 (Karimi et al., 2002) for the expression of C-terminal GFP fusions under the control of the native promoter sequences or 35S promoter, respectively. For BiFC assays, coding sequences were mobilized into pDEST-VYNE(R)^{GW} and pDEST-VYCE(R)^{GW} to generate N-terminal fusions with the N- and C-terminal halves of VENUS, respectively. To generate *ProIQD:GFP-GUS* reporter constructs, the promoter region was mobilized into pBGWFS7 (Karimi et al., 2002).

Plant Transformation

For transient expression assays in *N. benthamiana*, leaves were coinfiltrated with *Agrobacterium tumefaciens* GV3101 pMP90RK harboring plasmids and the silencing suppressor p19 in a 1:1 ratio. Bacterial cultures were adjusted to an optical density at 600 nm of 0.5 using infiltration buffer, and *N. benthamiana* leaves were pressure infiltrated through the abaxial epidermis. *A. tumefaciens*-mediated transient transformation of Arabidopsis was performed in leaves of 4-week-old plants grown under short-day conditions according to the protocol described by Mangano et al. (2014). For stable transformation of Arabidopsis, the floral dip technique was used (Clough and Bent, 1998), and eight to 24 independent transgenic lines were identified in the T1 generation by Basta selection for each construct analyzed. To verify single-copy transgene insertion, T2 transgenic lines were analyzed for a 3:1 segregation ratio (Basta). GFP fluorescence and GUS expression were analyzed in homozygous T3 plants of two to four lines showing representative GUS expression patterns or growth phenotypes.

Quantitative Real-Time PCR and RT-PCR

Rosette leaves from three individual 4-week-old plants were pooled, and total RNA was extracted from approximately 100 mg of tissue using the RNeasy Plant

Mini Kit (Qiagen). After DNase treatment, first-strand cDNA was synthesized from 4 μg of RNA using oligo(dT) primers with the Revert Aid First Strand cDNA synthesis kit (Thermo Fisher). Quantitative real-time PCR was performed on the 7500 Fast Real-Time PCR system using Fast SYBR Green master mix (Applied Biosystems) with 2 μL of 1:10 diluted cDNA. The relative expression of *IQD16* was calculated relative to *PP2A*. For RT-PCR analyses, RNA was isolated from 5-d-old seedlings grown under sterile conditions, and cDNA was synthesized from 5 μg of total RNA as described above. *ACTIN2* was amplified from 2 μL of 1:10 diluted cDNA, and 2 μL of undiluted cDNA was used as a template for the amplification of *IQD16* and *IQD25*. Primers used for amplification and their sequences are given in Supplemental Tables S3 and S4.

Histochemical Analysis

For GUS staining, sample tissues were fixed in 80% (v/v) ice-cold acetone for 30 min and incubated for 2 to 8 h in GUS staining solution [50 mM sodium phosphate, pH 7.2, 0.5 mM $K_3Fe(CN)_6$, 0.5 mM $K_4Fe(CN)_6$, 2 mM 5-bromo-4-chloro-3-indolyl-β-glucuronic acid, 10 mM EDTA, and 0.1% (v/v) Triton X-100] at 37°C. Imaging of GUS staining patterns was performed using a Zeiss Axioplan 2 microscope.

Confocal Laser Scanning Microscopy

Unless stated otherwise, imaging was performed with a Zeiss LSM 700 inverted microscope using a 40× water-immersion objective. The excitation wavelength for GFP and YFP was 488 nm; emission was detected between 493 and 555 nm. RFP was excited with a 555-nm laser, and emission was detected using a long-pass filter (582–700). For colocalization assays, images were obtained in the sequential mode. Root cells of transgenic Arabidopsis seedlings were plasmolyzed by treatment with 150 mM NaCl as described by Müller et al. (2015). For PI or FM4-64 staining, cells were incubated for 1 to 5 min in 10 μM PI or 50 μM Synapto-Red C2, respectively. Seedlings were imaged after two wash steps in sterile water. For the analysis of epidermis pavement cell shapes, single optical sections of the adaxial side of FM4-64-stained cotyledons were acquired with a 20× objective. Surface images of epidermal cells were acquired with a 63× water-immersion objective. BiFC assays were carried out with a Zeiss LSM 710 inverted microscope according to the protocol described by Gehl et al. (2009). Imaging was performed with identical laser settings for all samples, and emission spectra of reconstituted fluorescence were recorded by lambda scan.

Oryzalin treatments were performed as described by Bürstenbinder et al. (2013). Briefly, a 2 mM stock solution of oryzalin was prepared in dimethyl sulfoxide. *N. benthamiana* leaf discs were incubated in an aqueous solution of 50 μM oryzalin for up to 90 min. For treatment of Arabidopsis seedlings, plants were incubated in a final concentration of 20 μM oryzalin for 1 to 3 h.

Image Analysis

For semiautomatic segmentation, cell outlines were labeled in the red channel by PI staining or by expressing PM-localized RFP-PDLP1 (Amari et al., 2010). In maximum projections, cell outlines appear as thin vessel-like structures with locally varying contrast. The contrast was optimized by smoothing of the image with a Gaussian filter ($\sigma = 1$) and applying a Mexican hat filter in 18 steps of 10° to emphasize vessel-like structures. The resulting images containing the maximal filter response for each pixel were binarized by local Niblack thresholding as implemented in MiToBo (Möller et al., 2016). Subsequently, postprocessing steps were applied to the binary images (i.e. component labeling, exclusion of too-small components, and skeletonization), which allowed the extraction of large parts of the cell boundaries. Remaining gaps were corrected by manual postprocessing, and cells exceeding the image border were excluded manually. Subsequently, texture analysis techniques were applied to automatically characterize MT organization as stated in the result section of the main text (see Fig. 5). The feature vectors of all cells were jointly clustered applying k means. For each cell, the ratio of windows belonging to the different k clusters was calculated, which results in a k dimensional cluster distribution vector. Each cluster refers to a specific structural pattern appearing in the cells; hence, each vector can be interpreted as a probability density distribution of these patterns appearing in the corresponding cell. From the set of vectors, pairwise distances or distances between average vectors for each cell line were extracted and visualized in heat maps or adjacency networks (Fig. 3, A and B). The plots shown in this study were generated by applying nonoverlapping windows with a size of 16 × 16 pixels from which rotation invariant local binary patterns were extracted. For clustering, k was set to 10 and Euclidean distances were used. These parameters were empirically determined in prestudies that revealed that changing of parameters (i.e. window size and sliding windows) did not affect the detected global tendencies. In total, the analysis was based on 130 images containing 184 cells. For each IQD family member, five to 14 individual cells were analyzed. Networks were visualized with Cytoscape (Shannon et al., 2003).

To assess the lateral mobility of membrane subdomains, stacks of 10 to 12 images were acquired over 20 min in intervals of 2 min. Lateral shift of stacks was corrected via the Fiji plugin Stackreg (Schindelin et al., 2012). Kymographs were generated with the Fiji command Reslice using a line width of 12.

Quantification of subdomains was performed with Fiji. Images were background subtracted (rolling ball, 70 pixels). The radius was set according to the heuristically determined maximal size of objects of interest. Dot structures were detected with the wavelet-based particle detector (Greß et al., 2010) included in the MiToBo toolbox (jmin = 3, jmax = 5, scale interval of s = 2). The correlation threshold was fixed to t = 0.6, and regions with sizes between 100 and 1,750 pixels were analyzed to calculate average domain sizes.

Epidermis pavement cell shape was analyzed in cotyledons of 5-d-old seedlings grown sterile under long-day conditions. Cell walls were visualized by PI staining. Cell outlines were labeled in single optical sections of epidermis pavement cells with Fiji, and margin roughness and eccentricity were calculated as measures of (non)smoothness of the contour and cellular elongation, respectively. As a measure of cell shape (ir)regularity, first an average angle of tangent orientation changes is computed along the cell contour based on tangent orientations of pairs of adjacent contour points. Next, the deviation of the calculated angle from the angle expected for a perfect circle with an equal number of sampling points is calculated, referred to as margin roughness. A higher margin roughness value corresponds to a higher degree of nonsmoothness and reflects the extent of cellular lobing. Eccentricity is defined as the ratio between the extension of a region along its main axis and along the corresponding perpendicular axis. The extension along each axis is extracted from second-order central moments of the cell region. An almost circular region has an eccentricity value of 0, which increases with increasing elongation.

Immunocytochemistry

For ultrastructural localization of GFP-tagged proteins, root tips were transferred into aluminum planchettes and high-pressure frozen with an HPM 10 apparatus (Bal-Tec). Subsequently, the material was cryosubstituted in 0.25% (v/v) glutaraldehyde (Sigma) and 0.1% (w/v) uranyl acetate (Chemapol) in acetone for 2 d at −80°C using cryosubstitution equipment (FSU; Bal-Tec). This was followed by embedding in HM20 (Polysciences Europe) at −20°C.

For immunolabeling of ultrathin sections, we used a polyclonal anti-GFP antibody (600-101-215; Rockland) detected by a rabbit anti-goat secondary antibody conjugated with 10-nm gold (G 5527; Sigma). Sections were poststained with uranyl acetate and lead citrate in an EM-Stain apparatus (Leica) and subsequently observed with an EM 900 transmission electron microscope (Carl Zeiss Microscopy). Micrographs were taken with the Variospeed SSCCD (TRS).

Statistical Analysis

Statistical analysis was performed in R (version 3.2.1) by one-way ANOVA with Tukey's honestly significant difference test.

Accession Numbers

Sequence data from this article can be found in the GenBank/EMBL data libraries under accession numbers At3g09710 (IQD1), At5g03040 (IQD2), At3g52290 (IQD3), At2g26410 (IQD4), At3g22190 (IQD5), At2g26180 (IQD6), At1g17480 (IQD7), At1g72670 (IQD8), At2g33990 (IQD9), At3g15050 (IQD10), At5g13460 (IQD11), At5g03960 (IQD12), At3g59690 (IQD13), At2g43680 (IQD14), At3g49380 (IQD15), At4g10640 (IQD16), At4g00820 (IQD17), At1g01110 (IQD18), At4g14750 (IQD19), At3g51380 (IQD20), At3g49260 (IQD21), At4g23060 (IQD22), At5g62070 (IQD23), At5g07240 (IQD24), At4g29150 (IQD25), At3g16490 (IQD26), At1g51960 (IQD27), At1g14380 (IQD28), At2g02790 (IQD29), At1g18840 (IQD30), At1g74690 (IQD31), At1g19870 (IQD32), At5g35670 (IQD33), At5g19780 (TUA5), At5g43980 (PDLP1), At3g02170 (TRM1), At1g13920 (Rem6.6), At5g61280 (Rem6.7), At3g18780 (ACTIN2), At1g13320 (PP2Ac), At2g41110 (CaM2).

Supplemental Data

The following supplemental materials are available.

Supplemental Figure S1. Expression analysis and subcellular localization of Arabidopsis *IQD* genes.

Supplemental Figure S2. Phenotypes of *iqd25* mutant lines and expression analysis of *ProIQD25*::*GFP-GUS*.

Supplemental Figure S3. Phenotypes of *iqd16* lines and expression analysis of *ProIQD16*::*GFP-GUS*.

Supplemental Figure S4. Expression analysis of *IQD11* and *IQD14* overexpression lines and of *ProIQD11*:*GFP-GUS* and *ProIQD14*:*GFP-GUS* lines.

Supplemental Figure S5. Coexpression assays of GFP-IQD fusions with RFP-CaM2.

Supplemental Figure S6. Predicted properties of Arabidopsis IQD proteins.

Supplemental Table S1. Prediction of nuclear localization signals, lipidation sites, and signal peptides in Arabidopsis IQD proteins.

Supplemental Table S2. Gene identifiers and plasmids.

Supplemental Table S3. Primer combinations used for quantitative PCR, RT-PCR, and genotyping.

Supplemental Table S4. Primer sequences.

ACKNOWLEDGMENTS

We thank Petra Dietrich for CaM pENTR clones.

Received November 14, 2016; accepted January 20, 2017; published January 23, 2017.

LITERATURE CITED

Abel S, Bürstenbinder K, Müller J (2013) The emerging function of IQD proteins as scaffolds in cellular signaling and trafficking. Plant Signal Behav **8:** e24369

Abel S, Savchenko T, Levy M (2005) Genome-wide comparative analysis of the *IQD* gene families in *Arabidopsis thaliana* and *Oryza sativa*. BMC Evol Biol **5:** 72

Amari K, Boutant E, Hofmann C, Schmitt-Keichinger C, Fernandez-Calvino L, Didier P, Lerich A, Mutterer J, Thomas CL, Heinlein M, et al (2010) A family of plasmodesmal proteins with receptor-like properties for plant viral movement proteins. PLoS Pathog **6:** e1001119

Babu MM, van der Lee R, de Groot NS, Gsponer J (2011) Intrinsically disordered proteins: regulation and disease. Curr Opin Struct Biol **21:** 432–440

Benschop JJ, Mohammed S, O'Flaherty M, Heck AJR, Slijper M, Menke FLH (2007) Quantitative phosphoproteomics of early elicitor signaling in Arabidopsis. Mol Cell Proteomics **6:** 1198–1214

Bigeard J, Rayapuram N, Bonhomme L, Hirt H, Pflieger D (2014) Proteomic and phosphoproteomic analyses of chromatin-associated proteins from Arabidopsis thaliana. Proteomics **14:** 2141–2155

Bisgrove SR, Lee YR, Liu B, Peters NT, Kropf DL (2008) The microtubule plus-end binding protein EB1 functions in root responses to touch and gravity signals in *Arabidopsis*. Plant Cell **20:** 396–410

Bringmann M, Landrein B, Schudoma C, Hamant O, Hauser MT, Persson S (2012) Cracking the elusive alignment hypothesis: the microtubule-cellulose synthase nexus unraveled. Trends Plant Sci **17:** 666–674

Bürstenbinder K, Savchenko T, Müller J, Adamson AW, Stamm G, Kwong R, Zipp BJ, Dinesh DC, Abel S (2013) Arabidopsis calmodulin-binding protein IQ67-domain 1 localizes to microtubules and interacts with kinesin light chain-related protein-1. J Biol Chem **288:** 1871–1882

Buschmann H, Dols J, Kopischke S, Peña EJ, Andrade-Navarro MA, Heinlein M, Szymanski DB, Zachgo S, Doonan JH, Lloyd CW (2015) Arabidopsis KCBP interacts with AIR9 but stays in the cortical division zone throughout mitosis via its MyTH4-FERM domain. J Cell Sci **128:** 2033–2046

Buschmann H, Fabri CO, Hauptmann M, Hutzler P, Laux T, Lloyd CW, Schäffner AR (2004) Helical growth of the Arabidopsis mutant *tortifolia1* reveals a plant-specific microtubule-associated protein. Curr Biol **14:** 1515–1521

Cárdenas L (2009) New findings in the mechanisms regulating polar growth in root hair cells. Plant Signal Behav **4:** 4–8

Charpentier M, Oldroyd GE (2013) Nuclear calcium signaling in plants. Plant Physiol **163:** 496–503

Chen X, Wu S, Liu Z, Friml J (2016) Environmental and endogenous control of cortical microtubule orientation. Trends Cell Biol **26:** 409–419

Clough SJ, Bent AF (1998) Floral dip: a simplified method for *Agrobacterium*-mediated transformation of *Arabidopsis thaliana*. Plant J **16:** 735–743

Craddock C, Lavagi I, Yang ZB (2012) New insights into Rho signaling from plant ROP/Rac GTPases. Trends Cell Biol **22:** 492–501

Deavours BE, Reddy AS, Walker RA (1998) Ca^{2+}/calmodulin regulation of the Arabidopsis kinesin-like calmodulin-binding protein. Cell Motil Cytoskeleton **40:** 408–416

Deeks MJ, Calcutt JR, Ingle EKS, Hawkins TJ, Chapman S, Richardson AC, Mentlak DA, Dixon MR, Cartwright F, Smertenko AP, et al (2012) A superfamily of actin-binding proteins at the actin-membrane nexus of higher plants. Curr Biol **22:** 1595–1600

Demir F, Horntrich C, Blachutzik JO, Scherzer S, Reinders Y, Kierszniowska S, Schulze WX, Harms GS, Hedrich R, Geiger D, et al (2013) Arabidopsis nanodomain-delimited ABA signaling pathway regulates the anion channel SLAH3. Proc Natl Acad Sci USA **110:** 8296–8301

Dodd AN, Kudla J, Sanders D (2010) The language of calcium signaling. Annu Rev Plant Biol **61:** 593–620

Drevensek S, Goussot M, Duroc Y, Christodoulidou A, Steyaert S, Schaefer E, Duvernois E, Grandjean O, Vantard M, Bouchez D, et al (2012) The *Arabidopsis* TRM1-TON1 interaction reveals a recruitment network common to plant cortical microtubule arrays and eukaryotic centrosomes. Plant Cell **24:** 178–191

Endler A, Persson S (2011) Cellulose synthases and synthesis in Arabidopsis. Mol Plant **4:** 199–211

Feng L, Chen Z, Ma H, Chen X, Li Y, Wang Y, Xiang Y (2014) The *IQD* gene family in soybean: structure, phylogeny, evolution and expression. PLoS ONE **9:** e110896

Filiz E, Tombuloglu H, Ozyigit II (2013) Genome-wide analysis of IQ67 domain (IQD) gene families in *Brachypodium distachyon*. Plant Omics **6:** 425–432

Fischer C, Kugler A, Hoth S, Dietrich P (2013) An IQ domain mediates the interaction with calmodulin in a plant cyclic nucleotide-gated channel. Plant Cell Physiol **54:** 573–584

Furutani I, Watanabe Y, Prieto R, Masukawa M, Suzuki K, Naoi K, Thitamadee S, Shikanai T, Hashimoto T (2000) The SPIRAL genes are required for directional control of cell elongation in Arabidopsis thaliana. Development **127:** 4443–4453

Gardiner J (2013) The evolution and diversification of plant microtubule-associated proteins. Plant J **75:** 219–229

Gehl C, Waadt R, Kudla J, Mendel RR, Hänsch R (2009) New GATEWAY vectors for high throughput analyses of protein-protein interactions by bimolecular fluorescence complementation. Mol Plant **2:** 1051–1058

Goldenberg NM, Steinberg BE (2010) Surface charge: a key determinant of protein localization and function. Cancer Res **70:** 1277–1280

Graham LE (1996) Green algae to land plants: an evolutionary transition. J Plant Res **109:** 241–251

Greß O, Möller B, Stöhr N, Hüttelmaier S, Posch S (2010) Scale-adaptive wavelet-based particle detection in microscopy images. *In* Proceedings of Workshop Bildverarbeitung für die Medizin. Springer, Heidelberg, Germany, pp 266–270

Gutierrez R, Lindeboom JJ, Paredez AR, Emons AM, Ehrhardt DW (2009) Arabidopsis cortical microtubules position cellulose synthase delivery to the plasma membrane and interact with cellulose synthase trafficking compartments. Nat Cell Biol **11:** 797–806

Hamada T, Nagasaki-Takeuchi N, Kato T, Fujiwara M, Sonobe S, Fukao Y, Hashimoto T (2013) Purification and characterization of novel microtubule-associated proteins from Arabidopsis cell suspension cultures. Plant Physiol **163:** 1804–1816

Hashimoto K, Kudla J (2011) Calcium decoding mechanisms in plants. Biochimie **93:** 2054–2059

Hemsley PA, Grierson CS (2008) Multiple roles for protein palmitoylation in plants. Trends Plant Sci **13:** 295–302

Hemsley PA, Weimar T, Lilley KS, Dupree P, Grierson CS (2013) A proteomic approach identifies many novel palmitoylated proteins in Arabidopsis. New Phytol **197:** 805–814

Hepler PK (1992) Calcium and mitosis. Int Rev Cytol **138:** 239–268

Hepler PK (2005) Calcium: a central regulator of plant growth and development. Plant Cell **17:** 2142–2155

Hepler PK (2016) The cytoskeleton and its regulation by calcium and protons. Plant Physiol **170:** 3–22

Huang Z, Van Houten J, Gonzalez G, Xiao H, van der Knaap E (2013) Genome-wide identification, phylogeny and expression analysis of *SUN, OFP* and *YABBY* gene family in tomato. Mol Genet Genomics **288:** 111–129

Hülskamp M, Misŕa S, Jürgens G (1994) Genetic dissection of trichome cell development in Arabidopsis. Cell **76:** 555–566

Humphrey TV, Haasen KE, Aldea-Brydges MG, Sun H, Zayed Y, Indriolo E, Goring DR (2015) PERK-KIPK-KCBP signalling negatively regulates root growth in Arabidopsis thaliana. J Exp Bot **66:** 71–83

Idilli AI, Morandini P, Onelli E, Rodighiero S, Caccianiga M, Moscatelli A (2013) Microtubule depolymerization affects endocytosis and exocytosis in the tip and influences endosome movement in tobacco pollen tubes. Mol Plant **6:** 1109–1130

Ishida T, Kaneko Y, Iwano M, Hashimoto T (2007) Helical microtubule arrays in a collection of twisting tubulin mutants of *Arabidopsis thaliana*. Proc Natl Acad Sci USA **104:** 8544–8549

Ivakov A, Persson S (2013) Plant cell shape: modulators and measurements. Front Plant Sci **4:** 439

Jarsch IK, Konrad SSA, Stratil TF, Urbanus SL, Szymanski W, Braun P, Braun KH, Ott T (2014) Plasma membranes are subcompartmentalized into a plethora of coexisting and diverse microdomains in *Arabidopsis* and *Nicotiana benthamiana*. Plant Cell **26:** 1698–1711

Jurado LA, Chockalingam PS, Jarrett HW (1999) Apocalmodulin. Physiol Rev **79:** 661–682

Kao YL, Deavours BE, Phelps KK, Walker RA, Reddy AS (2000) Bundling of microtubules by motor and tail domains of a kinesin-like calmodulin-binding protein from Arabidopsis: regulation by Ca^{2+}/calmodulin. Biochem Biophys Res Commun **267:** 201–207

Karimi M, Inzé D, Depicker A (2002) GATEWAY vectors for *Agrobacterium*-mediated plant transformation. Trends Plant Sci **7:** 193–195

Kirik V, Herrmann U, Parupalli C, Sedbrook JC, Ehrhardt DW, Hülskamp M (2007) CLASP localizes in two discrete patterns on cortical microtubules and is required for cell morphogenesis and cell division in Arabidopsis. J Cell Sci **120:** 4416–4425

Kong Z, Ioki M, Braybrook S, Li S, Ye ZH, Julie Lee YR, Hotta T, Chang A, Tian J, Wang G, et al (2015) Kinesin-4 functions in vesicular transport on cortical microtubules and regulates cell wall mechanics during cell elongation in plants. Mol Plant **8:** 1011–1023

Konrad SS, Popp C, Stratil TF, Jarsch IK, Thallmair V, Folgmann J, Marín M, Ott T (2014) S-Acylation anchors remorin proteins to the plasma membrane but does not primarily determine their localization in membrane microdomains. New Phytol **203:** 758–769

Konrad SSA, Ott T (2015) Molecular principles of membrane microdomain targeting in plants. Trends Plant Sci **20:** 351–361

Kosugi S, Hasebe M, Matsumura N, Takashima H, Miyamoto-Sato E, Tomita M, Yanagawa H (2009) Six classes of nuclear localization signals specific to different binding grooves of importin alpha. J Biol Chem **284:** 478–485

Kudla J, Batistic O, Hashimoto K (2010) Calcium signals: the lead currency of plant information processing. Plant Cell **22:** 541–563

Kudla J, Bock R (2016) Lighting the way to protein-protein interactions: recommendations on best practices for bimolecular fluorescence complementation analyses. Plant Cell **28:** 1002–1008

Kusumi A, Fujiwara TK, Chadda R, Xie M, Tsunoyama TA, Kalay Z, Kasai RS, Suzuki KG (2012) Dynamic organizing principles of the plasma membrane that regulate signal transduction: commemorating the fortieth anniversary of Singer and Nicolson's fluid-mosaic model. Annu Rev Cell Dev Biol **28:** 215–250

Lee YK, Kim GT, Kim IJ, Park J, Kwak SS, Choi G, Chung WI (2006) *LONGIFOLIA1* and *LONGIFOLIA2*, two homologous genes, regulate longitudinal cell elongation in *Arabidopsis*. Development **133:** 4305–4314

Levy M, Wang Q, Kaspi R, Parrella MP, Abel S (2005) *Arabidopsis* IQD1, a novel calmodulin-binding nuclear protein, stimulates glucosinolate accumulation and plant defense. Plant J **43:** 79–96

Lincoln C, Britton JH, Estelle M (1990) Growth and development of the *axr1* mutants of *Arabidopsis*. Plant Cell **2:** 1071–1080

Lindeboom JJ, Nakamura M, Hibbel A, Shundyak K, Gutierrez R, Ketelaar T, Emons AM, Mulder BM, Kirik V, Ehrhardt DW (2013) A mechanism for reorientation of cortical microtubule arrays driven by microtubule severing. Science **342:** 1245533

Liu Z, Persson S, Zhang Y (2015) The connection of cytoskeletal network with plasma membrane and the cell wall. J Integr Plant Biol **57:** 330–340

Liu Z, Schneider R, Kesten C, Zhang Y, Somssich M, Zhang Y, Fernie AR, Persson S (2016) Cellulose-microtubule uncoupling proteins prevent lateral displacement of microtubules during cellulose synthesis in Arabidopsis. Dev Cell **38:** 305–315

Lloyd C, Hussey P (2001) Microtubule-associated proteins in plants: why we need a MAP. Nat Rev Mol Cell Biol **2:** 40–47

Lucas JR, Courtney S, Hassfurder M, Dhingra S, Bryant A, Shaw SL (2011) Microtubule-associated proteins MAP65-1 and MAP65-2 positively regulate axial cell growth in etiolated *Arabidopsis* hypocotyls. Plant Cell **23:** 1889–1903

Ma H, Feng L, Chen Z, Chen X, Zhao H, Xiang Y (2014) Genome-wide identification and expression analysis of the IQD gene family in Populus trichocarpa. Plant Sci **229:** 96–110

Malinsky J, Opekarová M, Grossmann G, Tanner W (2013) Membrane microdomains, rafts, and detergent-resistant membranes in plants and fungi. Annu Rev Plant Biol **64:** 501–529

Mangano S, Gonzalez CD, Petruccelli S (2014) *Agrobacterium tumefaciens*-mediated transient transformation of *Arabidopsis thaliana* leaves. Methods Mol Biol **1062:** 165–173

Marc J, Granger CL, Brincat J, Fisher DD, Kao T, McCubbin AG, Cyr RJ (1998) A GFP-MAP4 reporter gene for visualizing cortical microtubule rearrangements in living epidermal cells. Plant Cell **10:** 1927–1940

Marchand V, Gaspar I, Ephrussi A (2012) An intracellular transmission control protocol: assembly and transport of ribonucleoprotein complexes. Curr Opin Cell Biol **24:** 202–210

McCormack E, Braam J (2003) Calmodulins and related potential calcium sensors of *Arabidopsis*. New Phytol **159:** 585–598

McCormack E, Tsai YC, Braam J (2005) Handling calcium signaling: Arabidopsis CaMs and CMLs. Trends Plant Sci **10:** 383–389

Mishima M, Maesaki R, Kasa M, Watanabe T, Fukata M, Kaibuchi K, Hakoshima T (2007) Structural basis for tubulin recognition by cytoplasmic linker protein 170 and its autoinhibition. Proc Natl Acad Sci USA **104:** 10346–10351

Möller B, Glaß M, Misiak D, Posch S (2016) MiToBo: a toolbox for image processing and analysis. J Open Res Softw **4:** e17

Möller B, Piltz E, Bley N (2014) Quantification of actin structures using unsupervised pattern analysis techniques. Proc Int Conf Pattern Recognition ICPR 14, IEEE, 3251–3256

Müller J, Toev T, Heisters M, Teller J, Moore KL, Hause G, Dinesh DC, Bürstenbinder K, Abel S (2015) Iron-dependent callose deposition adjusts root meristem maintenance to phosphate availability. Dev Cell **33:** 216–230

Nakagawa T, Suzuki T, Murata S, Nakamura S, Hino T, Maeo K, Tabata R, Kawai T, Tanaka K, Niwa Y, et al (2007) Improved Gateway binary vectors: high-performance vectors for creation of fusion constructs in transgenic analysis of plants. Biosci Biotechnol Biochem **71:** 2095–2100

Narasimhulu SB, Reddy AS (1998) Characterization of microtubule binding domains in the *Arabidopsis* kinesin-like calmodulin binding protein. Plant Cell **10:** 957–965

Nigg EA (1997) Nucleocytoplasmic transport: signals, mechanisms and regulation. Nature **386:** 779–787

Ojala T, Pietikainen M, Maenpaa T (2002) Multiresolution gray-scale and rotation invariant texture classification with local binary patterns. IEEE T Pattern Anal **24:** 971–987

Oppenheimer DG, Pollock MA, Vacik J, Szymanski DB, Ericson B, Feldmann K, Marks MD (1997) Essential role of a kinesin-like protein in Arabidopsis trichome morphogenesis. Proc Natl Acad Sci USA **94:** 6261–6266

Palm D, Simm S, Darm K, Weis BL, Ruprecht M, Schleiff E, Scharf C (2016) Proteome distribution between nucleoplasm and nucleolus and its relation to ribosome biogenesis in Arabidopsis thaliana. RNA Biol **13:** 441–454

Raffaele S, Mongrand S, Gamas P, Niebel A, Ott T (2007) Genome-wide annotation of remorins, a plant-specific protein family: evolutionary and functional perspectives. Plant Physiol **145:** 593–600

Reddy AS, Ben-Hur A, Day IS (2011) Experimental and computational approaches for the study of calmodulin interactions. Phytochemistry **72:** 1007–1019

Ren J, Wen L, Gao X, Jin C, Xue Y, Yao X (2008) CSS-Palm 2.0: an updated software for palmitoylation sites prediction. Protein Eng Des Sel **21:** 639–644

Roll-Mecak A (2015) Intrinsically disordered tubulin tails: complex tuners of microtubule functions? Semin Cell Dev Biol **37:** 11–19

Saka SK, Honigmann A, Eggeling C, Hell SW, Lang T, Rizzoli SO (2014) Multi-protein assemblies underlie the mesoscale organization of the plasma membrane. Nat Commun **5:** 4509

Schindelin J, Arganda-Carreras I, Frise E, Kaynig V, Longair M, Pietzsch T, Preibisch S, Rueden C, Saalfeld S, Schmid B, et al (2012) Fiji: an open-source platform for biological-image analysis. Nat Methods **9:** 676–682

Scholl RL, May ST, Ware DH (2000) Seed and molecular resources for Arabidopsis. Plant Physiol **124:** 1477–1480

Scott AM, Antal CE, Newton AC (2013) Electrostatic and hydrophobic interactions differentially tune membrane binding kinetics of the C2 domain of protein kinase Cα. J Biol Chem **288:** 16905–16915

Sedbrook JC, Ehrhardt DW, Fisher SE, Scheible WR, Somerville CR (2004) The *Arabidopsis sku6/spiral1* gene encodes a plus end-localized microtubule-interacting protein involved in directional cell expansion. Plant Cell **16:** 1506–1520

Sedbrook JC, Kaloriti D (2008) Microtubules, MAPs and plant directional cell expansion. Trends Plant Sci **13:** 303–310

Shahbabian K, Chartrand P (2012) Control of cytoplasmic mRNA localization. Cell Mol Life Sci **69:** 535–552

Shannon KB (2012) IQGAP family members in yeast, Dictyostelium, and mammalian cells. Int J Cell Biol **2012:** 894817

Shannon P, Markiel A, Ozier O, Baliga NS, Wang JT, Ramage D, Amin N, Schwikowski B, Ideker T (2003) Cytoscape: a software environment for integrated models of biomolecular interaction networks. Genome Res **13:** 2498–2504

Sheahan MB, Staiger CJ, Rose RJ, McCurdy DW (2004) A green fluorescent protein fusion to actin-binding domain 2 of Arabidopsis fimbrin highlights new features of a dynamic actin cytoskeleton in live plant cells. Plant Physiol **136:** 3968–3978

Shoji T, Narita NN, Hayashi K, Asada J, Hamada T, Sonobe S, Nakajima K, Hashimoto T (2004) Plant-specific microtubule-associated protein SPIRAL2 is required for anisotropic growth in Arabidopsis. Plant Physiol **136:** 3933–3944

Smith JM, Hedman AC, Sacks DB (2015) IQGAPs choreograph cellular signaling from the membrane to the nucleus. Trends Cell Biol **25:** 171–184

Smith LG, Gerttula SM, Han S, Levy J (2001) Tangled1: a microtubule binding protein required for the spatial control of cytokinesis in maize. J Cell Biol **152:** 231–236

Spira F, Mueller NS, Beck G, von Olshausen P, Beig J, Wedlich-Söldner R (2012) Patchwork organization of the yeast plasma membrane into numerous coexisting domains. Nat Cell Biol **14:** 640–648

Steinhorst L, Kudla J (2013) Calcium: a central regulator of pollen germination and tube growth. Biochim Biophys Acta **1833:** 1573–1581

Struk S, Dhonukshe P (2014) MAPs: cellular navigators for microtubule array orientations in Arabidopsis. Plant Cell Rep **33:** 1–21

Tian J, Han L, Feng Z, Wang G, Liu W, Ma Y, Yu Y, Kong Z (2015) Orchestration of microtubules and the actin cytoskeleton in trichome cell shape determination by a plant-unique kinesin. eLife **4:** 4

Tompa P, Davey NE, Gibson TJ, Babu MM (2014) A million peptide motifs for the molecular biologist. Mol Cell **55:** 161–169

Toufighi K, Brady SM, Austin R, Ly E, Provart NJ (2005) The Botany Array Resource: e-northerns, expression angling, and promoter analyses. Plant J **43:** 153–163

van der Knaap E, Chakrabarti M, Chu YH, Clevenger JP, Illa-Berenguer E, Huang Z, Keyhaninejad N, Mu Q, Sun L, Wang Y, et al (2014) What lies beyond the eye: the molecular mechanisms regulating tomato fruit weight and shape. Front Plant Sci **5:** 227

Vavouri T, Semple JI, Garcia-Verdugo R, Lehner B (2009) Intrinsic protein disorder and interaction promiscuity are widely associated with dosage sensitivity. Cell **138:** 198–208

Wang L, Li H, Lv X, Chen T, Li R, Xue Y, Jiang J, Jin B, Baluška F, Šamaj J, et al (2015) Spatiotemporal dynamics of the BRI1 receptor and its regulation by membrane microdomains in living Arabidopsis cells. Mol Plant **8:** 1334–1349

Wang YC, Wang BC, Gilroy S, Chehab EW, Braam J (2011) CML24 is involved in root mechanoresponses and cortical microtubule orientation in Arabidopsis. J Plant Growth Regul **30:** 467–479

Wang YS, Motes CM, Mohamalawari DR, Blancaflor EB (2004) Green fluorescent protein fusions to Arabidopsis fimbrin 1 for spatio-temporal imaging of F-actin dynamics in roots. Cell Motil Cytoskeleton **59:** 79–93

Wright PE, Dyson HJ (2015) Intrinsically disordered proteins in cellular signalling and regulation. Nat Rev Mol Cell Biol **16:** 18–29

Wu M, Li Y, Chen D, Liu H, Zhu D, Xiang Y (2016) Genome-wide identification and expression analysis of the IQD gene family in moso bamboo (Phyllostachys edulis). Sci Rep **6:** 24520

Wu S, Xiao H, Cabrera A, Meulia T, van der Knaap E (2011) SUN regulates vegetative and reproductive organ shape by changing cell division patterns. Plant Physiol **157:** 1175–1186

Xiao H, Jiang N, Schaffner E, Stockinger EJ, van der Knaap E (2008) A retrotransposon-mediated gene duplication underlies morphological variation of tomato fruit. Science **319:** 1527–1530

Xie Y, Zheng Y, Li H, Luo X, He Z, Cao S, Shi Y, Zhao Q, Xue Y, Zuo Z, et al (2016) GPS-Lipid: a robust tool for the prediction of multiple lipid modification sites. Sci Rep **6:** 28249

Yang T, Poovaiah BW (2003) Calcium/calmodulin-mediated signal network in plants. Trends Plant Sci **8:** 505–512

Zárský V, Cvrcková F, Potocký M, Hála M (2009) Exocytosis and cell polarity in plants: exocyst and recycling domains. New Phytol **183:** 255–272

Zentella R, Zhang ZL, Park M, Thomas SG, Endo A, Murase K, Fleet CM, Jikumaru Y, Nambara E, Kamiya Y, et al (2007) Global analysis of DELLA direct targets in early gibberellin signaling in *Arabidopsis*. Plant Cell **19:** 3037–3057

Zhu C, Ganguly A, Baskin TI, McClosky DD, Anderson CT, Foster C, Meunier KA, Okamoto R, Berg H, Dixit R (2015a) The Fragile Fiber1 kinesin contributes to cortical microtubule-mediated trafficking of cell wall components. Plant Physiol **167:** 780–792

Zhu X, Dunand C, Snedden W, Galaud JP (2015b) CaM and CML emergence in the green lineage. Trends Plant Sci **20:** 483–489